Research Report
Agreement T1461, Task 78
WSDOT Expansion Joint Ph 2

DESIGN AND TESTING OF MODULAR EXPANSION JOINT NOISE MITIGATION STRATEGIES

by

Per Reinhall, Professor
Jeff Lipton, Assistant Professor
Sawyer Thomas, Graduate Research Assistant
Waiel Elmadih, Research Scientist

University of Washington
Department of Mechanical Engineering

Washington State Transportation Center (TRAC)
University of Washington, Box 359446
University Tower
4333 Brooklyn Ave NE
Seattle, Washington 98195-8690

Washington State Department of Transportation
Technical Monitor Mark Gaines

Prepared for

The State of Washington
Department of Transportation
Roger Millar, Secretary

December 2022

TECHNICAL REPORT STANDARD TITLE PAGE

. REPORT NO.	2. GOVERNMENT ACCESSION NO.	3. RECIPIENT'S CATALOG NO.
WA-RD 920.1		

4. TITLE AND SUBTITLE	5. REPORT DATE
Design and Testing of Modular Expansion Joint Noise Mitigation Strategy	December 2022
	6. PERFORMING ORGANIZATION CODE
7. AUTHOR(S)	8. PERFORMING ORGANIZATION REPORT NO.
Per Reinhall, Sawyer Thomas, Jeff Lipton, Waiel Elmadih	
9. PERFORMING ORGANIZATION NAME AND ADDRESS Washington State Transportation Center (TRAC) University of Washington, Box 359446 University Tower; 4333 Brooklyn Ave NE Seattle, Washington 98195-8690	10. WORK UNIT NO.
	11. CONTRACT OR GRANT NO. Agreement T1461, Task 78
12. SPONSORING AGENCY NAME AND ADDRESS Research Office Washington State Department of Transportation Transportation Building, MS 47372 Olympia, Washington 98504-7372 Project Manager: Jon Peterson, 360.705.7499	13. TYPE OF REPORT AND PERIOD COVERED Research Report
	14. SPONSORING AGENCY CODE

15. SUPPLEMENTARY NOTES

This study was conducted in cooperation with the U.S. Department of Transportation, Federal Highway Administration.

16. ABSTRACT:

This study investigated the design and feasibility of noise mitigation strategies for installation in modular expansion joints (MEJs), with a focus on Washington state's SR 520 bridge. The three main sources of noise from MEJs include resonance of the air within the gaps, resonance of the beams, and resonance of the tires. By filling the gaps in the MEJs with engineered chevron support structures we have shown that it is feasible to significantly reduce the noise from MEJs. We performed both experimental and computer evaluations of a noise attenuation system before performing limited testing on the SR 520 bridge.

Installation of the treatment on one westbound lane of the east MEJ of the SR 520 bridge proved to be highly effective over the two-month test period. At a distance of 160 feet, we measured a more than 70 percent reduction in audible noise over the noise of background traffic throughout the testing period. Beyond 160 feet the difference between noise from the concrete road surface and from the MEJ became so small that it became very difficult to identify when individual cars crossed the MEJ. While we have shown that the chevron system can be an effective solution to the expansion joint noise issue, we outline further development and testing to extend the durability of the treatment.

17. KEY WORDS	18. DISTRIBUTION STATEMENT
	No restrictions. This document is available to the public through the National Technical Information Service, Springfield, VA 22616

19. SECURITY CLASSIF. (of this report)	20. SECURITY CLASSIF. (of this page)	21. NO. OF PAGES	22. PRICE
None	None		

Disclaimer

The contents of this report reflect the views of the authors, who are responsible for the facts and the accuracy of the data presented herein. The contents do not necessarily reflect the official views or policies of the Washington State Department of Transportation or Federal Highway Administration. This report does not constitute a standard, specification, or regulation.

Americans with Disabilities Act (ADA) Information

In accordance with the requirements of Title II of the Americans with Disabilities Act of 1990, the Washington State Department of Transportation (WSDOT) will not discriminate against qualified individuals with disabilities on the basis of disability in its services, programs, or activities. WSDOT is committed to providing programs, services, and activities that are in compliance with Title II of the Americans with Disabilities Act of 1990 and Section 504 and 508 of the Rehabilitation Act of 1973.

This material can be made available in an alternate format by emailing the Office of Equal Opportunity at wsdotada@wsdot.wa.gov or by calling toll free, 855-362-4ADA(4232). Persons who are deaf or hard of hearing may make a request by calling the Washington State Relay at 711.

Title VI Notice to Public

It is the Washington State Department of Transportation's (WSDOT's) policy to assure that no person shall, on the grounds of race, color, or national origin, as provided by Title VI of the Civil Rights Act of 1964, be excluded from participation in, be denied the benefits of, or be otherwise discriminated against under any of its programs and activities. Any person who believes their Title VI protection has been violated, may file a complaint with WSDOT's Office of Equal Opportunity (OEO). For additional information regarding Title VI complaint procedures and/or information regarding our non-discrimination obligations, please contact OEO's Title VI Coordinator at (360) 705-7090.

Notificación de Titulo VI al Público

Es la política del Departamento de Transportación del Estado de Washington (WSDOT, por sus siglas en inglés) asegurarse que ninguna persona, por razón de raza, color, origen, nacionalidad, según provee el Título VI de la Ley de Derechos Civiles de 1964, pueda ser

excluido de la participación, negado los beneficios de o ser discriminado de otra manera bajo cualquiera de sus programas y actividades. Cualquier persona que crea que su protección bajo el Titulo VI ha sido violada, puede presentar una queja o reclamación ante la Oficina de Igualdad de Oportunidades (OEO, por sus siglas en inglés) del Departamento de Transportación del Estado de Washignton (WSDOT, por sus siglas en inglés). Para obtener información adicional sobre los procedimientos de quejas y/o reclamaciones bajo el Titulo VI y/o información sobre nuestras obligaciones anti-discriminatorias, pueden contactar al coordinador del Título VI en la EEOC 360-705-7090.

Información de la Ley sobre Estadounidenses con Discapacidades
(ADA, por sus siglas en inglés)

Este material está disponible en un formato alternativo, que puede ser solicitado al enviar un un correo electrónico a la Oficina de Igualdad de Oportunidades (OEO, por sus siglas en inglés)/ wsdotada@wsdot.wa.gov o llamando gratis al siguiente número de teléfono: 855-362-4ADA (4232). Personas sordas o con discapacidad auditiva pueden solicitar la misma información llamando al Washington State Relay al 711.

Table of Contents

Figures

Table

Executive Summary

As required in ESSB 5689, Section 219 (4), this study investigated the design and feasibility of noise mitigation strategies for installation in modular expansion joints (MEJs), with a focus on Washington state's SR 520 bridge. The three main sources of noise from MEJs include resonance of the air within the gaps, resonance of the beams, and resonance of the tires. By filling the gaps in the MEJs with engineered chevron support structures, we showed that it is feasible to significantly reduce the noise from MEJs. We performed both experimental and computer evaluations of a noise attenuation system before performing limited testing on the SR 520 bridge.

Installation of the treatment on one westbound lane of the east MEJ of the SR 520 bridge proved to be highly effective over the two-month test period. At a distance of 160 feet, we measured a more than 70 percent reduction in audible noise over the noise of background traffic throughout the testing period. Beyond 160 feet the difference between noise from the concrete road surface and from the MEJ became so small that it became very difficult to identify when individual cars crossed the MEJ. While we have shown that the chevron system can be an effective solution to the expansion joint noise issue, we outline further development and testing to extend the durability of the treatment.

1. Introduction

Bridge and viaduct expansion joints play a critical role worldwide by enabling movement of the structure with changing environmental conditions. Expansion joints can be found on bridges around the world, each with specific designs, dimensions, and materials (see Figure 1-1). However, they all share the same concept: they connect two isolated sections of a bridge to provide a continuous medium for travellers[1]. The reason for having two isolated sections on the bridge in the first place is to make sure that expansion and contraction of the bridge due to changes in water level (for floating bridges), changes in temperature, lateral and rotational movement induced by wind and current, and general land movement do not cause any damage. The expansion allows motion to occur without causing excessive stress in the bridge that can lead to failure.

While expansion joints remain a necessary component for effective development, they also contribute to noise pollution and have become an area of focus for many acoustic studies and noise mitigation strategies[2–9]. Several potential technologies reduce expansion joint noise, such as sinus plates[1,10,11], foam inserts[8,12], and Helmholtz absorbers[6]; however, these solutions either require large-scale bridge renovation, fail to effectively reduce broadband noise, or require frequent maintenance. Here we suggest alternative sound mitigation strategies that show great potential for effectively retrofitting existing expansion joints.

Large modular expansion joints (MEJs) such as those installed on Washington state's Evergreen Point Floating Bridge (SR 520 bridge) tend to result in nuisance noise generation. Shortly after that bridge opened in 2016, the Washington State Department of Transportation (WSDOT) began receiving noise complaints related to the large expansion joints on the east and west ends of the bridge. The noticeable impact of each car hitting the MEJs contributes to noise pollution in the area. While this specific bridge has received complaints since its opening, similar expansion joints across the state and beyond pose similar difficulties associated with noise. To combat this problem, we developed, fabricated, and installed a test noise mitigation treatment in a single lane of the SR 520 floating bridge. Over the course of two months, we recorded and processed sound data to evaluate our results. Through this study, we gained significant insight into the mechanism and practical mitigation of MEJ noise.

1.1 The Modular Expansion Joint

To reduce the noise coming from the SR 520 bridge, we must consider the general design of the existing modular expansion joint (MEJ). The expansion joint consists of a closing box connected to a concrete block (one side of the bridge) and an opening box connected to the other side (Figure 1-1). A central beam runs between the boxes, leaving room toward the end of one box for expansion and contraction[13]. Supported on the central beam are the I-beams that protrude out of the sub-structures of the expansion joint, forming a travel surface with the rest of the bridge.

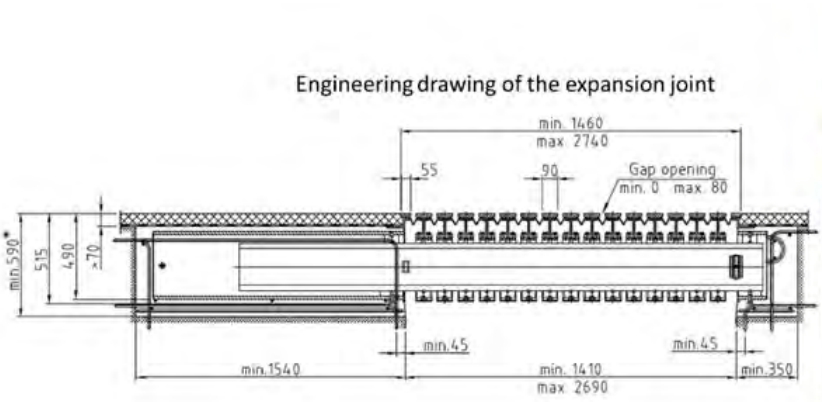

The main material used in the expansion joint is steel, with various hardening and grades in some critical regions, for example the shear studs that connect to the concrete. A gap exists between any two I-beams (including the edge beam and the first I-beam from each side). This gap changes width with the opening and closing of the expansion joint. A seal made of a flexible material (Neoprene) is mounted between each beam (below the surface of travel) to collect debris, dirt, water and/or any parts/particles that can potentially cause damage to the substructure of the expansion joint, as well as to keep untreated water and debris from entering Lake Washington. A large, enclosed cavity exists underneath the expansion joint on the east side to provide noise reduction and easy access to the expansion joints for servicing and replacing parts.

1.2 The Source of Noise

The source of the noise was discussed in detail in our previous research report, "Modular Expansion Joint Noise Mitigation Study," which was prepared for WSDOT in January 2019. This report discussed that the noise emanating from expansion joints is due to the following:

- The acoustic resonances of the air cavity enclosed by the tire, seal, and beams.
- Motion of the beams as they are excited by the tires when they strike the edges of the beams.
- The deformation of the tires as they strike the beams.

Additional conclusions from the previous study include the following:

- The noise as evaluated by energy spectral density (ESD) at residential locations is highest between 400 Hz and 800 Hz. ESD at the bridge close to the expansion joint is also highest between 400 Hz and 800 Hz.
- Most of the noise radiates from **the top** of the modular expansion.
- The frequency characteristics of the noise for vehicle-pass events are closely related to vehicle tire width. The frequency peak for wider tires occurs at lower frequencies than that for narrower tires. This is a result of excitation of the air volume between the tire and the air gap between center beams.
- A concrete joint cavity enclosure (WSDOT design) under the east expansion bridge significantly reduces the noise coming from the underside of the bridge.
- Filling the gaps between the center beams could reduce the noise on the SR 520 bridge and other expansion joints.

Understanding the cause of the noise is critical for exploring potential solutions. The previous report from the University of Washington (UW) successfully showed the levels of noise at various frequencies. In general, noises can generate from various sources, and the literature would categorize these sources on the basis of various generation mechanisms (things like frequency ranges, type, and nature). In this work, we identified two main generation mechanisms. The first one is acoustic radiation from the tire and the beams when the tires hit the edge of the I-beam on the expansion joint. The second-generation mechanism is acoustic radiation from the sudden compression and expansion of the air within the cavity formed by the seal and the top part of any two neighboring I-beams when a tire passes over the cavity. This can be viewed as a type

of Helmholtz resonator phenomenon. The previous study found a generally inverse relationship between tire width and dominant frequency such that f_{peak} is the peak of the ESD and W_t is the width of the tire.

$$f_{peak} \propto \frac{1}{W_t}$$

We simulated the deformation of the tire and the excitation pressure on the MEJ I-beams (Figure 1-2) with the help of a finite element model (see details in section 3. Methodology) of the tire and section of the expansion joint. As a tire rolls across the joint, it drops into the gap between the MEJ I-beams. As it meets the leading edge of the next I-beam, the tire accelerates upward, creating a pressure spike and exciting the structure and tire (Figure 1-2). By adding a structure that resists vertical deformation in the gap, we can support the tire as it rolls overhead, reducing the distance that the tire drops and subsequently reducing the pressure spike between the tire and the I-beam.

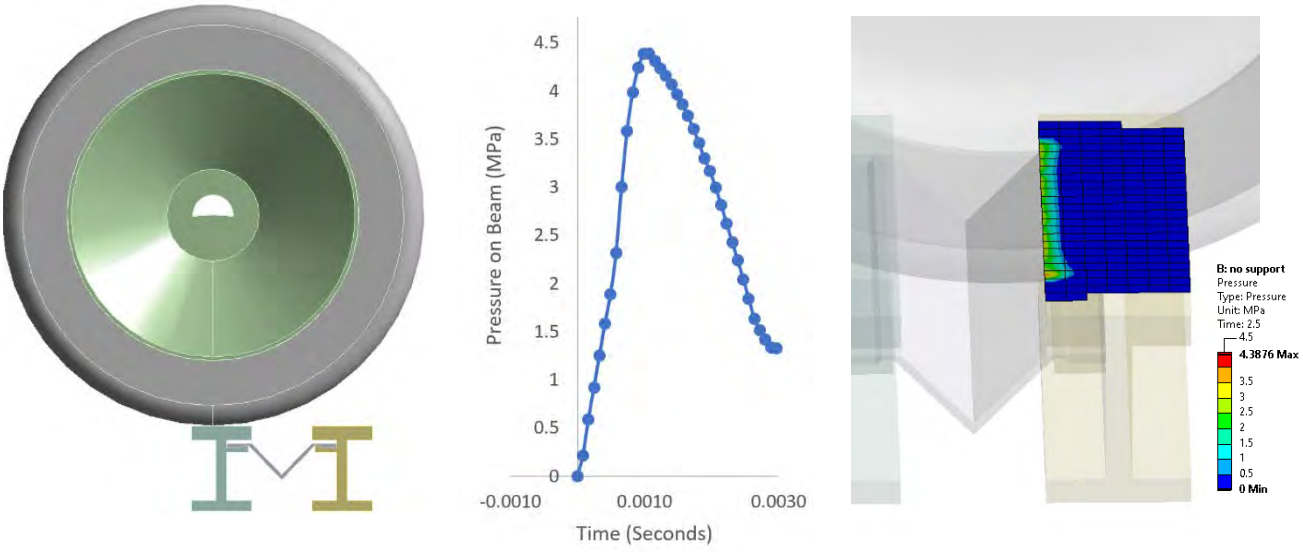

Figure 1-2. A) Computer aided design (CAD) model for the vehicle tire and I-beam design for simulation. B) A sharp pressure spike occurs as the tire rolls over the leading edge of the second I-beam. C) Visualization of peak pressure on the I-beam surface.

As a vehicle rolls over the expansion joint on the east side of the bridge, we observed in our measured noise data two distinct peaks in noise as each pair of tires (front and rear) strikes the beams of the MEJ. A third, smaller peak in noise occurs as the vehicle passes over a smaller joint slightly past the main joint. For testing, we considered a single event to be the time between the

front tires striking the first I-beam in the joint (Figure 1-3.B) and the vehicle completely passing the expansion joint (Figure 1-3.I). To evaluate smooth road noise, we sampled the audio directly before the vehicle rolled onto the expansion joint (before Figure 1-3.A)

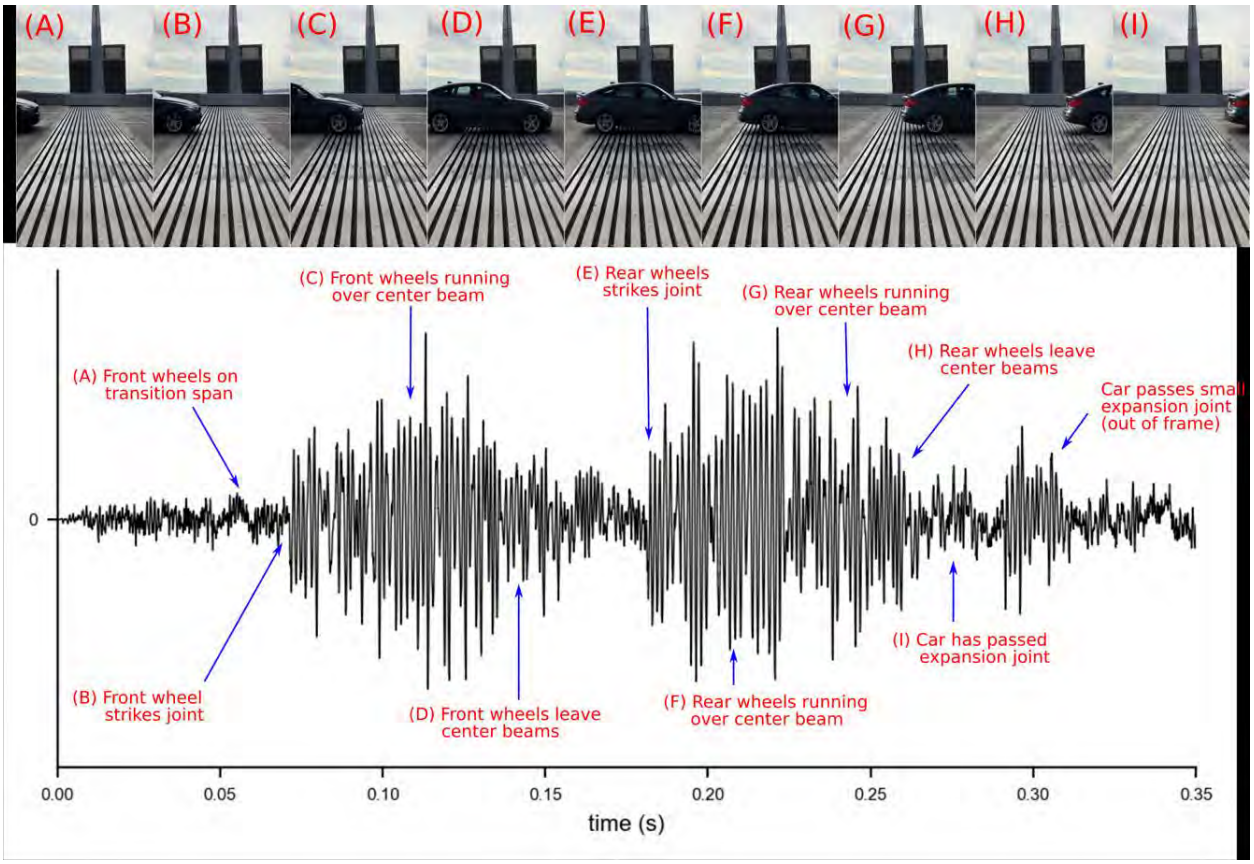

Figure 1-3. Overview of car-pass events using simultaneous noise and video recordings. Screenshots from high-speed video are assigned to specific parts of the noise recording using letters (A)-(I).

2. Noise Mitigation Design

2.1 Design Constraints

As described in our previous report, we must address three main noise generation mechanisms to create an effective noise mitigation treatment. These include 1) the vibration amplitude of the I-beams impacted by the tire, 2) the acoustic resonance amplitude of the air cavity under the tire, and 3) the noise emitted from the tire itself as it rolls across the MEJ. For each of these noise generation mechanisms, the exciting force is generated by the tire deforming into the gap between the beams as the tire crosses the expansion joint. By filling the space between each I-beam, we can reduce the amount by which the tire slips into the gaps, and as a result, limit pressure spikes in the beam, tire, and cavity simultaneously. To be effective, this treatment must partially be able to support the load of the tire while still allowing the joint to function as intended and surviving the wear of traffic and weather over time.

The geometric and structural constraints of the modular expansion joint create a challenging design problem. First, the structure must allow the MEJ to regularly open and close with gaps that shift between .84 in. to 3 in. during normal operation. The floating bridge has both vertical, rotational, and transverse movements up to 9 degrees that must be accounted for. Under extreme conditions the Pontoon "W" gap can potentially completely close to a 0-in. gap or expand to a width of 3.85 in. The pontoon “A” gap can expand to a width of 4.38 in. If the gap fully closes, the design must be easy to remove, or in a worst-case scenario the structure must selectively fail to allow full closure, ensuring that no damage occurs to the MEJ or bridge. Additionally, the solution should also be easy to install, durable, and include a moisture seal to prevent dirt, gravel, water, etc. from penetrating the substructure of the expansion joint or entering Lake Washington. These requirements necessitate a unique structure design that must have a horizontal expansion ratio of greater than 3.5 while still being able to partially support the weight of a semi-truck in the vertical direction. These designs must be extremely durable to withstand extended exposure to overhead roadway traffic and weather of all kinds.

2.2 Candidate Design Overview

To match the shifts in the beam gaps, the structure must expand and contract along the roadway with no material interference or height change along the length of the gap. To do this, our designs incorporate flexible chevrons tailored to have a net zero Poisson’s ratio behavior (Figure 2-1). This allows material to remain fastened in place and level with the roadway as the MEJ

expands and contracts over time. In between the I-beams, a neoprene moisture seal fastens to each beam via a welded metal connector (Figure 2-1). We explored two main design categories to retrofit the existing structure: 1) a single-layer design that we can install without removing the current moisture seal and 2) a multilayer support system with a custom fabricated moisture seal to replace the current version.

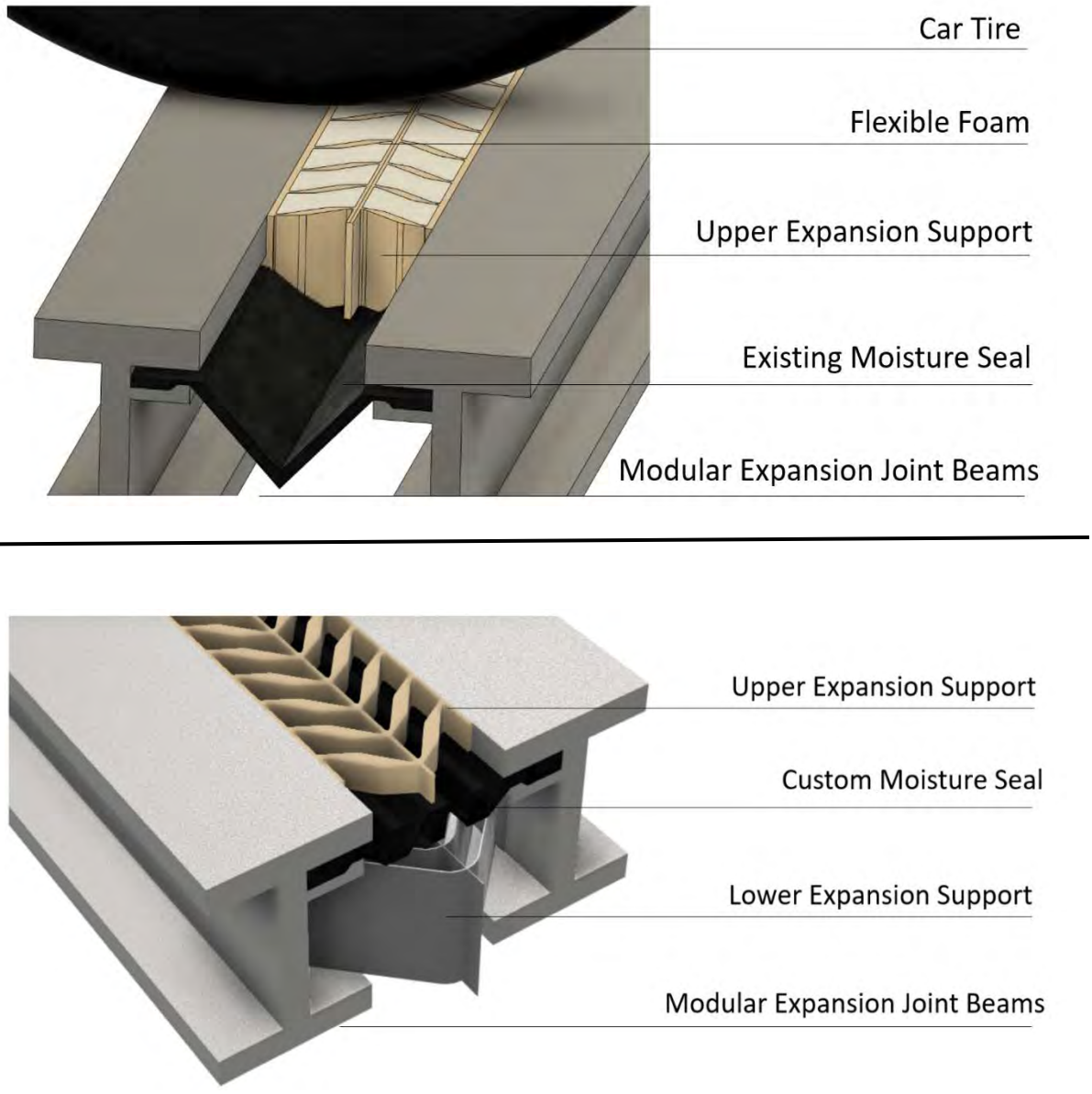

Figure 2-1. A) Single-layer elastomer chevron design with original moisture seal, installed between MEJ I-beams. B) Multi-layer design with an elastomer top layer and custom moisture seal.

2.3 Single-Layer Design

To offer the simplest solution, we propose retrofitting the existing MEJs such that no components need to be modified or replaced. To avoid altering the current moisture seal, we designed a support component that fits into the space accessible from the surface of the bridge. This support must be durable enough to withstand roadway wear and must compress/expand between .85 in. and 3 in. without yielding. Under extreme compression it must fail and squeeze out of the MEJ without causing any damage, meaning that rigid materials such as steel cannot be used. Rather than creating a traditional hinge design, which can be susceptible to blocking with grime and binding, we designed chevron structures with compliant flexure joints. These structures can be easily 3D printed or cast for prototyping and can eventually be injection molded for large-scale manufacturing. For installation, these can be easily compressed and inserted into the existing gaps.

To select the support shape, we created a chevron with the thickest beam and flexure width possible while still adhering to space limitations. To optimize material, we tapered the edge of each beam to neatly mesh with surrounding components during compression. This design relies on glued connections at each beam edge and small geometric interference between the moisture seal and the chevrons. For initial prototyping and testing, we fabricated these joints out of a variety of high durometer elastomers with shore hardness values between 85A-95A. For initial models, we 3D printed structures from Ninjatek–Cheetah thermoplastic polyurethane (TPU). These prototypes exhibited desirable traits, but fused deposition modelling (FDM) 3D printing could not be scaled to fabricate enough durable samples for our test on the SR 520 bridge. To create a larger number of high-quality durable parts, we instead switched from 3D printing to urethane casting. This process creates high quality parts with many high durability and commercial-grade options. We selected 90A durometer urethane from BJB Enterprises called FP90 A/B. With this material, our finite element models showed enough strength to tolerate complete compression of the structure within the MEJ's normal working limits (Figure 2-2). To test the structure's behavior in extreme conditions when the joint fully closed (a gap of 0 in.), we compressed a Ninjaflex chevron support using an Instron universal testing system with a force of 180 KN. This caused the support to squeeze to a final width of 0.164 in. and expand outward toward the edges of the test plates.

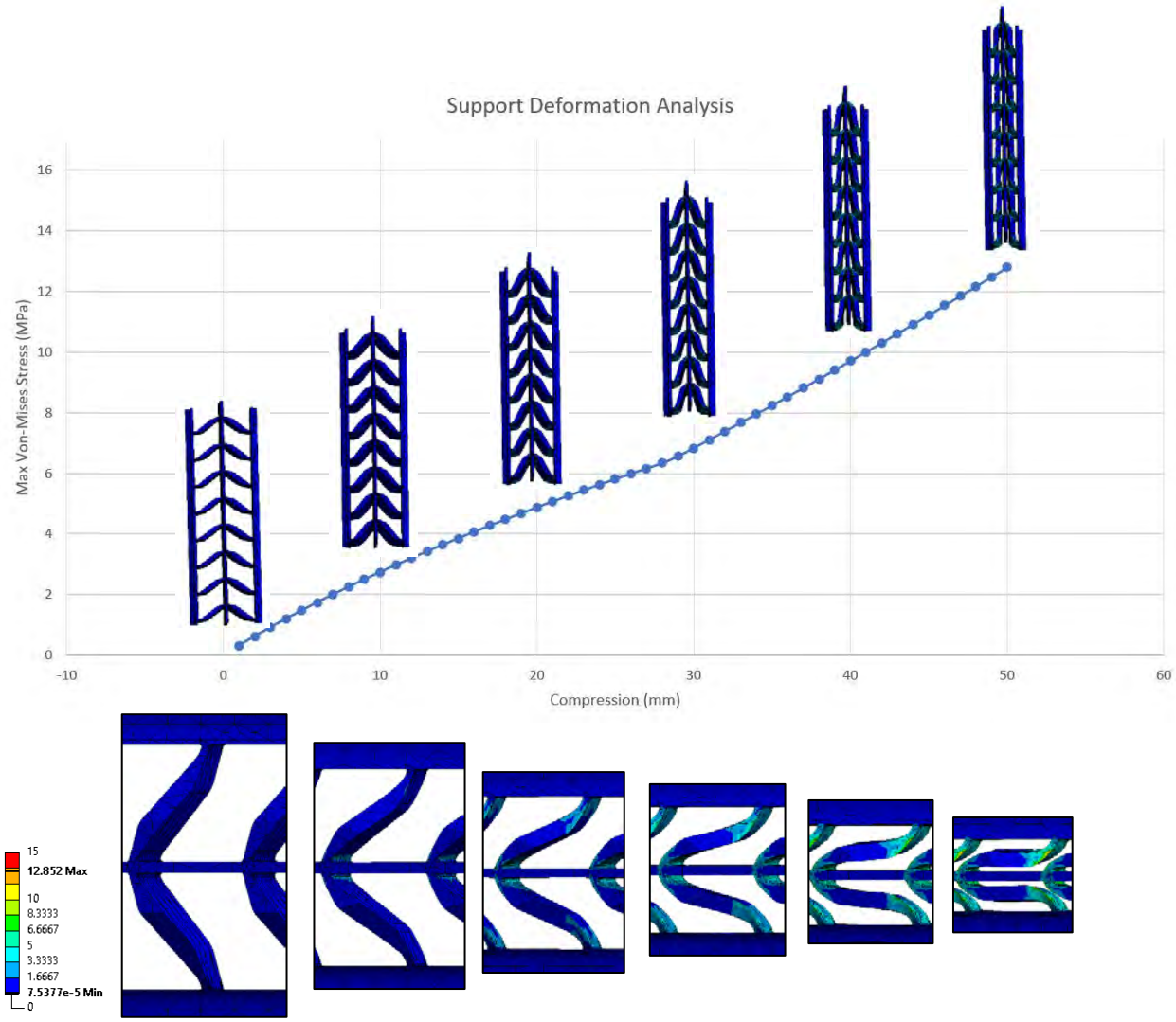

Figure 2-2. A) Plot of maximum internal stress as the support structure fully compresses. B) Detailed visualization of stress over the surface of each chevron element throughout

i

We performed the initial high-speed testing to assess the feasibility of different materials and geometry given a perfectly rigid lower support (roadway) (Figure 2-3). We investigated two potential material types: rigid plastic and semi rigid, high-durometer rubber (Appendix A) and performed tests at the PACCAR Facility in Mount Vernon, Washington. While these results demonstrated the feasibility of the supports in reducing noise in shallow roadway gaps, they also highlighted the importance of acoustic resonance in the cavities of the bridge structure. Even though we performed our testing on gap widths similar to those on the bridge, we recorded much lower noise levels on every configuration than those measured on the bridge. This indicated that that the resonance of the air cavities between the supports of the structure played a much larger

role than the magnitude of the tire and beam impacts. It was difficult to create an experimental set-up that closely resembled the true expansion joint. One issue was that the wooden ramps leading to the beams (Figure 2-3) created loud noises upon impact, making it difficult to process the data and draw detailed conclusions about the results. While we measured decreases in total noise with the added supports, background noise from the ramps made it difficult to confidently interpret the results.

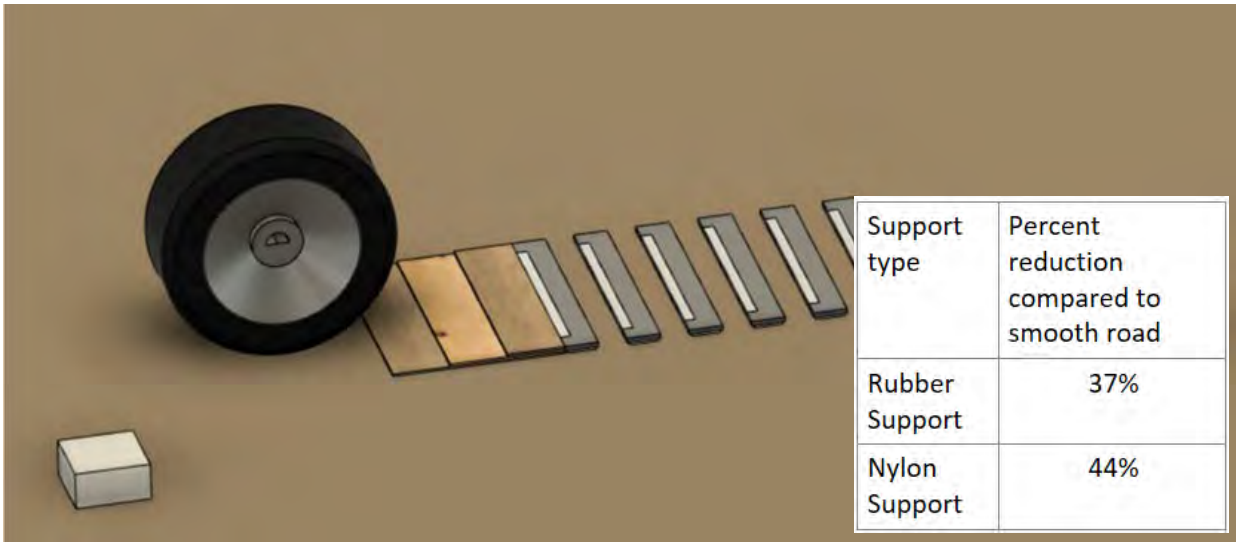

Support type	Percent reduction compared to smooth road
Rubber Support	37%
Nylon Support	44%

Figure 2-3. A) High speed test set-up. We made five 3-in. gaps by gluing a wooden ramp and 2-ft x 3.5-in. x75-in. metal beams to the roadway using a silicon-based glue. Two microphones sat before and after the test set-up to record noise (white boxes). B) Results showed slightly improved noise reduction with the more rigid material supporting the tire.

2.4 Multi-Layer Design

While the single-layer support design (Figure 2-1.A) benefits from simple fabrication and installation, an additional support layer could offer better resistance to deformation, potentially improving performance and reducing stress at glued connections (Figure 2-1.B). The bottom support structure rests in the I-beam cavity, supported by the lower flange of each I-beam. The lower support structure must repeatedly expand and compress between 5.875 in. and 2.875 in. to match the motion of MEJ Pontoon “W”; this offers significantly wider compression during the event of a fully closed joint than the upper support. Here, no possibility exists for the gap to fully close, so spring steel remains a viable material option. We designed two different support structures, a high-durometer urethane chevron and an interlocking, laser cut spring steel frame

(Figure 2-4). The urethane structure offers far less rigidity but could be injection molded or extruded for a low-cost solution.

We fabricated the elastomer structure by 3D printing molds and casting individual chevrons out of SmoothOn PMC 790 two-part urethane. We then glued overlapping portions to get a single connected structure. We ordered spring steel structure components to be laser cut and heat treated to improve elasticity. Notches in each sheet allowed easy assembly, and the chevrons attached to side plates with bolts (potentially rivets). For future installation, both structures may be installed by first clamping each section into a compressed state and dropping them into the gap, where they will be held in place by outward pressure. A layer of plastic siding must be included between the support and the beam to ensure no damage to the beam surface. To avoid interference with internal joint components such as nuts and bolts, the support must be selectively placed in small sections, potentially increasing installation time.

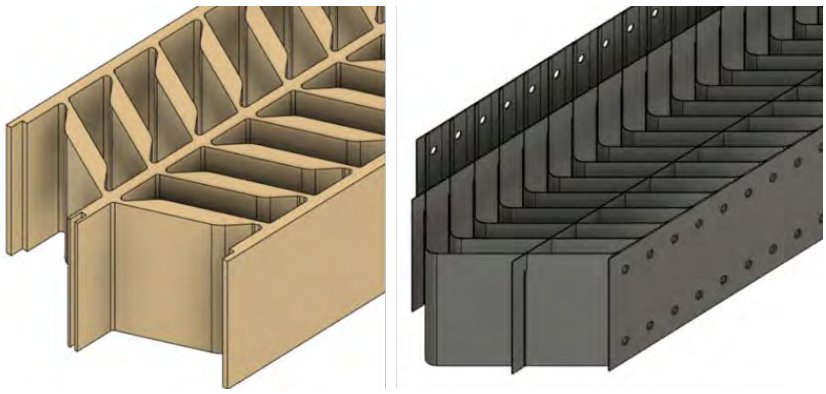

Figure 2-4. Bottom support structures. (Left) Chevron design fabricated from high durometer urethane. (Right) Structure fabricated from interlocking spring steel.

To validate our simulations and assess the potential of various multi-layer designs, we built a static compression test set-up (Figure 2-5) with reconfigurable components and tested eight different configurations for support deformation and edge pressure. To create realistic conditions, we fabricated I-beams matching those found on the SR 520 Bridge MEJ and drove a vehicle so that it rested on the installed supports. We used Fujifilm 70-350 psi Prescale pressure paper to determine edge pressure and an IFM diffuse light photoelectric distance sensor to measure deformation in the structure. On the physical MEJ, the largest tire deformations and subsequent impacts occur when the gap spans a larger distance. We positioned the I-beams accordingly to have a 3-in. gap, the maximum MEJ gap width within its normal working range. Every support

combination significantly reduced deformation in comparison to the untreated (unsupported) version. Between the two potential base supports, the spring steel version consistently performed far better than the urethan support, making it a strong candidate for future implementation.

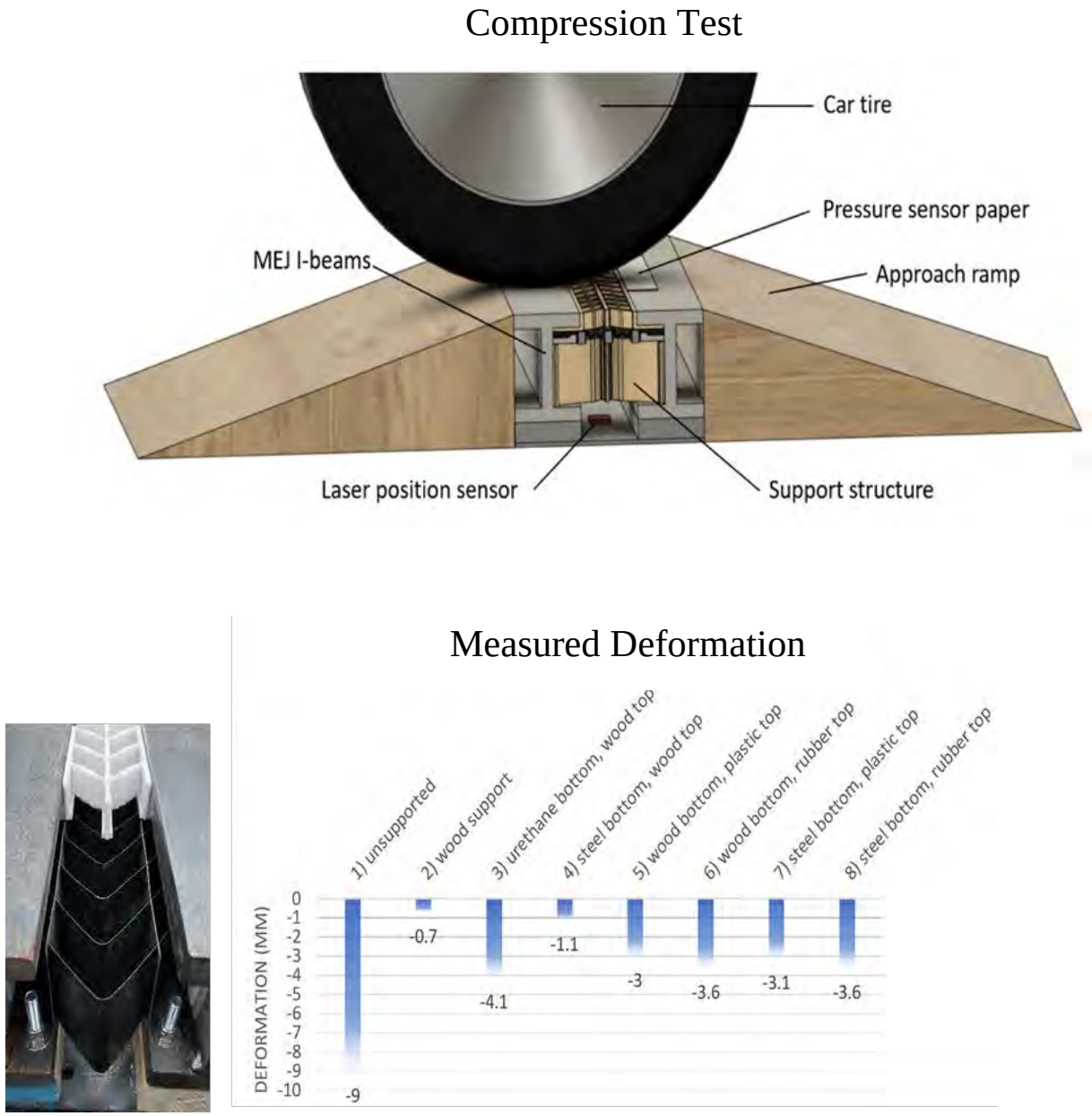

Figure 2-5. A) Set-up for static compression testing. B) Measured results from compression testing.

2.5 Design Selection

While both designs have potential to significantly reduce noise created by the Washington SR 520 modular expansion joints, we weighed practical considerations for implementing each support structure. We used finite element models to compare the influence of each on the resulting pressure spike caused by the tire on the beam edge. For the completely unsupported gap, the tire creates a sharp increase in pressure, with a peak of 4.39 MPa. For a perfectly flat road, the pressure of the tire rolling over the flat surface still creates a pressure spike but a much lower one, topping out at 1.45 MPa. If we consider the unsupported version to be the worst-case scenario, and the supported to be the best case, we can look at the percentage pressure reduction for each of the options.

$$\%\ Pressure\ Reduction = \frac{(P_{us} - P_{fs}) - (P_s - P_{fs})}{(P_{us} - P_{fs})}$$

with P_{us} being unsupported pressure, P_{fs} being flat surface pressure, and P_s being pressure of the support. Given the values shown in Figure 2-6, we see that the single-layer chevron support provided a pressure reduction of 67.17 percent, while the multi-layer chevron support (approximated as a rigid lower support) provided a pressure reduction of 76.40 percent. This may equate to driving over a slightly textured road as opposed to driving over a set of distinct metal beams such as a cattle guard. While the multi-layer support offered better reduction, both solutions provided significant improvements over the original unsupported beam gap. For these simulations, we focused specifically on the 3-in. beam gap configuration; a smaller gap may have shown lower overall values but would represent similar corresponding trends. In these simulations, we considered the connection between the support and the beams to be in contact. This connection relied on the surfaces to be bonded by either mechanical interference or a chemical adhesive. The multi-layer design did not rely as heavily on such a connection because of the support from below.

In addition to reducing pressure, each of the solutions deformed vertically and underwent internal stresses as vehicles rolled over top. For a 3-in. gap, the multi-layer support option had maximum internal stresses of 2.91 MPa and a surface deformation of 2.08 mm. The single-layer option had a significantly higher maximum stress of 4.64 MPa and a surface deformation of 3.60 mm. Stresses for both options were well below FP90's tensile strength of 14.5 MPa. The 3-in. gap represented the worst-case loading scenario; for smaller gaps we expect internal stresses to be reduced.

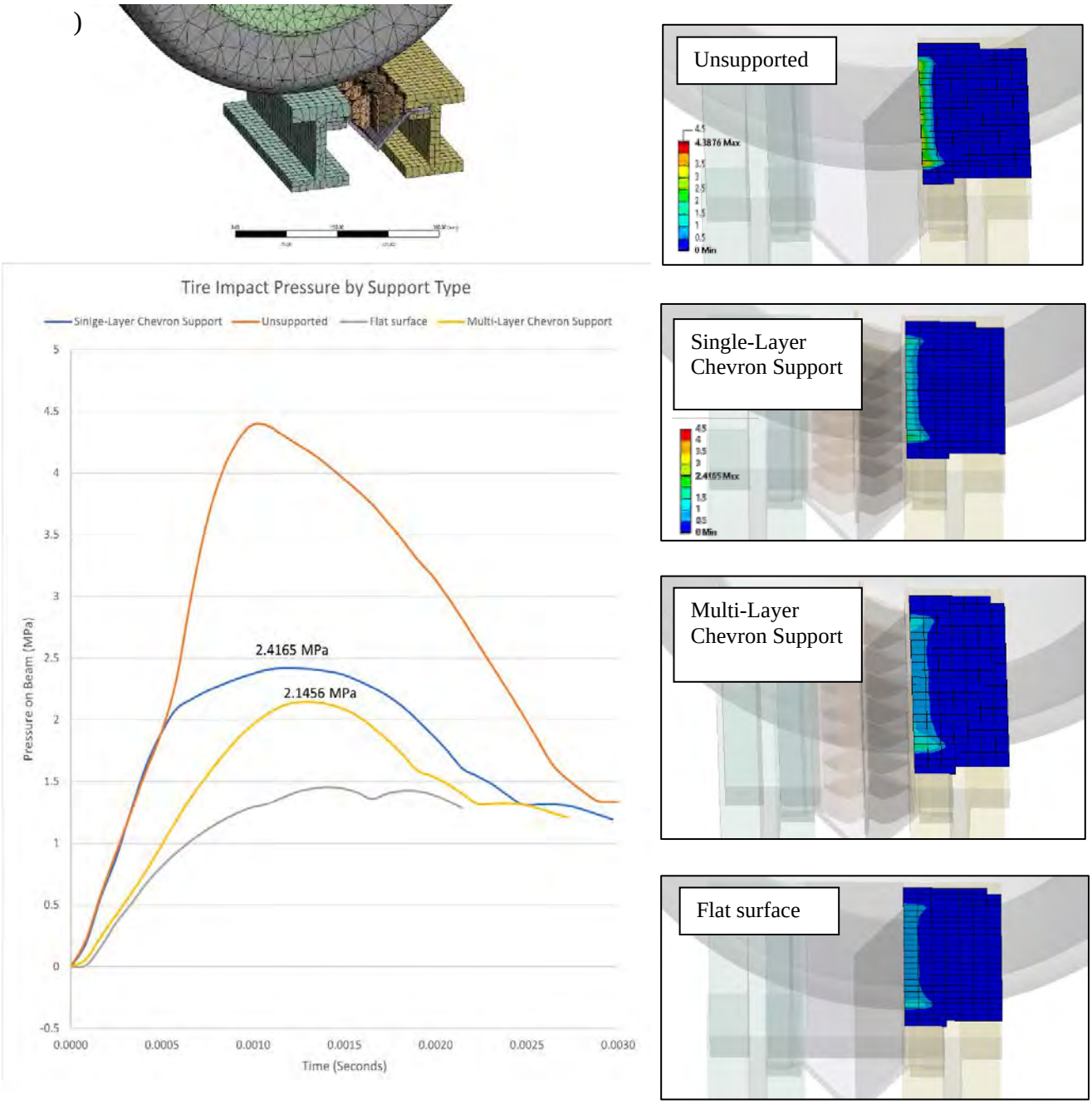

Figure 2-6. A) Mesh for the FEA of the rolling tire. B) Pressure curves as the tire strikes the leading edge of the second beam. C) Visualizations of the pressure on the edge of the beam for each treatment option.

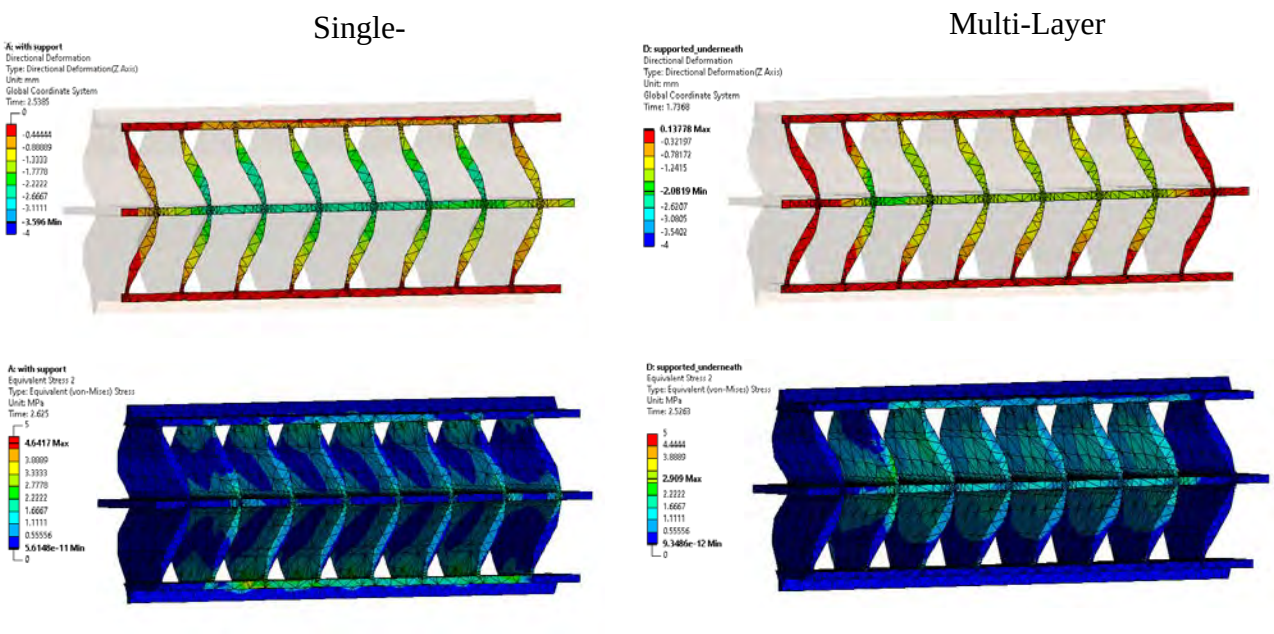

Figure 2-7. FEA visualizations of deformation of the top surface and internal stresses within the support as the tire rolls over the top.

Despite the slightly improved functionality of the multi-layer design, practical considerations favor installation of the single-layer design. Reducing the number of parts can drastically decrease the cost of fabrication and installation time. The reductions in internal stresses and pressures on beam edges are minimal in comparison to the benefits of simplicity. Along with analysis of the support structure, the adhesive and foam type for the single layer support structure also require careful consideration. Optimizing these materials will be critical to the long-term success of the treatment. To weigh the pros and cons of each solution, Table 2-1 summarizes significant points for each aspect of the design.

Given the points shown in the table, solution 1 (single-layer support) seems to be the best candidate for effective and affordable implementation. Solution 2 (multi-layer support) may provide increased resistance to deformation and reduce overall excitation of the system, but it requires far more complex and expensive fabrication and installation. For installation and field testing, we selected the single-layer support. Future work could investigate additional cost and durability trade-offs for a multi-layer support structure. Although the single-layer option seems like a better solution for retroactive installation, the multi-layer support could be potentially implemented in new bridge infrastructure.

Table 2-1: Key design points for multi-layer design vs single-layer design

Design Aspect	Single-Layer Design	Multi-Layer Design
Moisture seal replacement	Incorporates current moisture seal.	Required custom seal design, fabrication, and installation.
Structure Fabrication	Less complex fabrication that easily scales through urethane casting or injection molding.	Additional fabrication and assembly required for lower support.
Installation	Significantly simpler installation.	Multi-step installation required.
Pressure Reduction	Less reduction of pressure on the beam edge and impulse on the tire.	Higher reduction of pressure on beam and impulse on tire.
Durability	Less vertical support and greater reliance on beam edge contact.	Improved vertical support may lead to slightly better durability.

3. Methodology

3.1 Sound Equipment

Throughout this project, we used the same methodology and instruments used to complete the UW's phase 1 *Modular Expansion Joint Noise Mitigation Study*[14]. We took noise measurements with a Brüel and Kjaer Type 2270-S, class 1 (BK2270) sound level meter. We sampled acoustic data at a frequency of 48,000 Hz and recorded the files as 24-bit .wav files. We calibrated our files using a Brüel and Kjaer Type 4231 sound calibrator that outputs a 94±0.2 dB re 20 μPa tone at 1000 Hz.

3.2 Data Collection and Processing

Each sound level recording consisted of ~90 seconds of audio, during which many vehicles struck the modular expansion joint. To extract meaningful results from our sound measurements, we manually labelled events by selecting the start and end time of every vehicle that passed over the desired portion of the expansion joint. To do this, we compared matched video recordings to each audio recording to observe the specific time that each vehicle successfully struck the expansion joint segment in which our treatment was installed. To limit the influence of additional background noise, we selected only samples in which a single vehicle drove over the MEJ at a time. Additionally, we marked a short period (~.1 second) directly before the vehicle struck the expansion joint to act as a baseline measurement for comparison between the flat roadway and the MEJ for each vehicle. We used the open-source audio editor Audacity to mark and export text files with this information.

Next we computed the energy spectral density (ESD) to measure the associated spectra for each event[15,16]. This computation adapted the general method used during phase 1 of this project[14], and leveraged the SciPy. Signal toolbox[17] in Python to compute the power spectral density (PSD). We presented the ESD in dB with reference to E_{ref} of 1 $J/m^2/Hz$ (or 10 $log_{10}(ESD/E_{ref})$).

$$ESD = \frac{PSD \times T_e}{\rho c}$$

with T_e being event duration, ρ the density of air (1.225 kg/m^3), and c the speed of sound in air (340 m/s). For the ESD computation, we applied a Tukey (tapered-cosine) window with 25 percent tapering to the time series, and a Fast-Fourier Transform (FFT) zero padded to a length of

$4 \times f5$ (or 192,000 samples). Using a standard FFT length allowed spectral averages to be computed. It is important to note that ESD should not be confused with a pressure level widely used for measuring environmental noise. In comparing the ESD of two events, however, a higher ESD corresponds to a higher noise level. The Federal Highway Administration uses either 15-min or 1-hour equivalent sound levels, L_{eq}, and third-octave sound levels to measure compliance and noise abatement criteria. In this project we used ESD, as it allows transient events with varying durations to be compared. This is an effective tool to help investigate the mechanism(s) responsible for expansion joint noise, including their spectral characteristics, which was one of the main goals of this project. To apply a correction that accounted for the relative loudness of sounds perceived by the human ear, we applied A-weighting to some samples (SM). For these samples, ESD will be presented as dBA.

3.3 Simulation Information

3.3.1 Tire and Beam Model

We created a car tire model that approximated the complex geometry of a physical tire while preserving key characteristics. The computer aided design (CAD) model included a steel rim with an edge positioned directly at the center to act as pivot point for rolling. The model of the tire itself was made up of two layers. The interior layer represented a tire's inner liner, body plies, and the belts that give the tire structural strength. We approximated these as a 7-mm polyethylene strip with a Young's Modulus of 1.1 GPa and a Poisson's Ratio of 0.42. The outer layer represented the tire tread and sidewall. We modeled this as 18-mm thick rubber with a Young's Modulus of 20.6 MPa and a Poisson's ratio of 0.42. While this simple model only approximated the behavior of a tire, it functioned as an effective tool for comparing results between different treatment options. We modeled the MEJ beams as steel 1-foot extrusions of the I-beams used on the SR 520 Bridge. The moisture seal played no structural role in our simulations but was also approximated to be rubber like that of the tire.

3.3.2 Finite Element Model

To perform finite element analysis (FEA), we used the commercial software ANSYS Workbench 2021R1, a simulation suite for various types of solid and fluid analysis. For support compression and loading testing, we used ANSYS static structural simulation, with non-linear behavior and large deformations enabled. While this method only approximated the forces of a high-speed vehicle, it functioned as a useful tool for comparing several potential support

geometries. We applied bonded connections to each of the components in the tire and the beam assembly, respectively. Between the surface of the tire and the surface of the beams/supports, we created frictional contacts with a coefficient of friction of 0.2. We then generated a mesh by using ANSY's automatic mesh generation and a feature resolution of 6. To simulate the event of a car tire rolling over a gap in the beams, we broke the analysis into four separate steps.

1. First, we applied a displacement to one of the beams in the -Y direction to squeeze the support and establish the desired gap width and analyze stress in the chevron support joints.
2. Next, we applied a pressure of 35 PSI to the interior of the tire to effectively inflate the structure.
3. Third, we loaded the tire with -4448 N (1000 lbf) in the Z direction to approximate the weight of a medium-sized truck with equal force distributed on each tire.
4. Finally, we applied a remote displacement of 177 mm in the Y direction to roll the tire across the surface of the I-beam, into the gap, and onto the surface of the next I-beam.

To perform post-processing, we used the ANSYS contact tool to measure the pressure between the tire and the surface of the second beam over time. We also measured the displacement of the support surface and the stresses in the support throughout the simulation.

4. Results and Discussion

On the basis of our current installation of Solution 1 (Single-Layer Support) on the SR 520 Bridge Modular Expansion Joint, we present our experimental results and physical observations, as well as provide suggestions for future implementation.

4.1 Support Fabrication and Installation

For on-bridge testing, we ordered support structures cast from BJB Enterprises FP-90A urethane by Quickparts, a digital, on-demand manufacturing company. We ordered the chevrons in 6-in. segments with extending middle and edge sections to allow them to fit together. Before installation we used Loctite 406 instant adhesive to combine four 6-in. sections into 2-ft support strips. With proper application, this adhesive creates a strong bond between urethane rubbers; however, for future fabrication, support sections could be completely welded together with a more aggressive bonding method. To avoid directional biasing and transverse motion of the supports with repeated compression ("walking"), we joined the 2-ft sections so that each side included two 6-in. segments opposing each other (figures 4-1, 4-2).

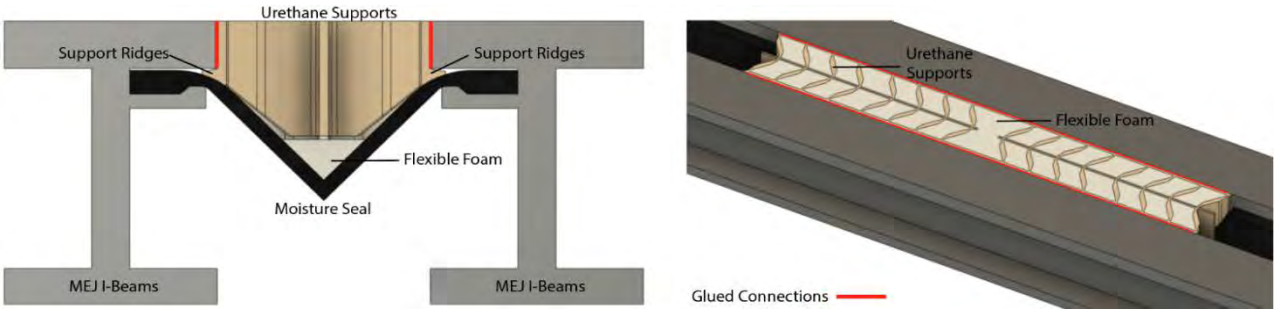

Figure 4-1. Diagram detailing support installation components.

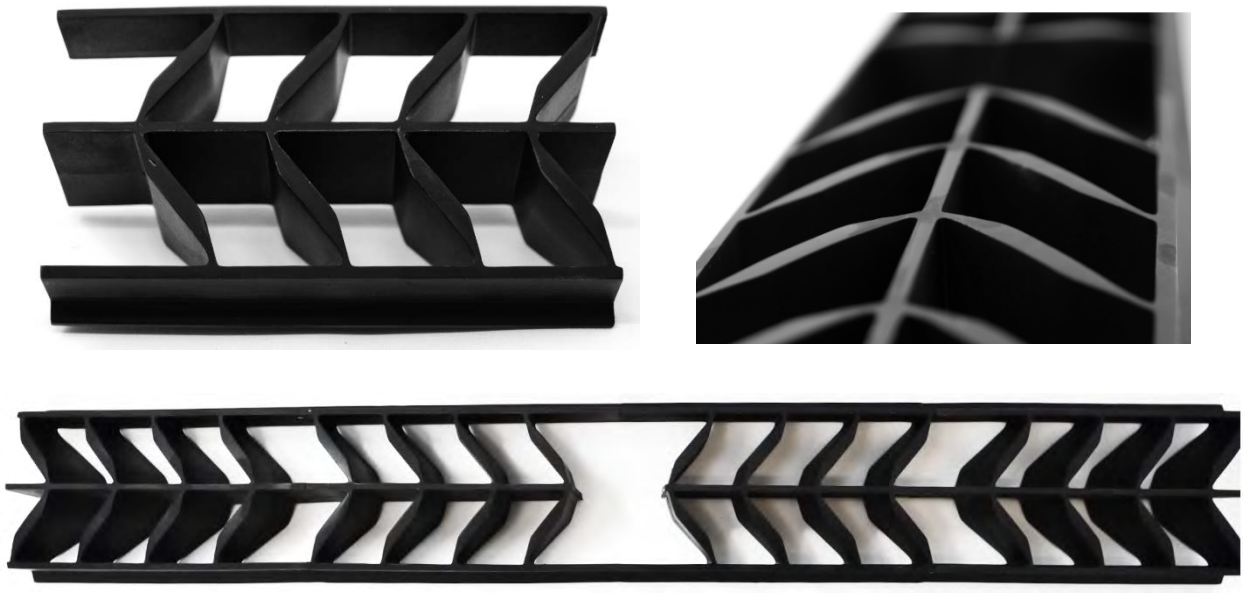

Figure 4-2. A) 6-in. sections of urethane cast support structures. B) We glued together four 6-inch support sections to create a single support with opposing direction chevrons.

For bridge installation, we first cleaned out a large amount of gravel and debris from the MEJ by using scraping tools and an air compressor. Next we cleaned the I-beam surface to glue the support to the edge. To secure the supports, we squeezed the sides by hand and slotted them into MEJ gaps so that the small ridges on the sides of the supports created mechanical interference with the edges of the moisture seal, locking them in place. Significant variation in the gap between the beam and the moisture seal made this step somewhat time consuming. To account for these variations, we manually trimmed some of the support ridges to create a tight fit. For future installation, an improved method of fitting these supports could greatly reduce installation time. We glued the support edges to the MEJ beam edges with Bostik 70-03A Elastic Bonding Adhesive.

Next we used 50-ml 2:1 ratio epoxy mixing guns to inject Smooth-On FlexFoam-iT III into each gap in the supports. This is a two-part flexible foam with a roughly 15x expansion ratio that is typically used for making soft cushions or props. While this foam acted as a good proof of concept for our design, a more durable selection of foam may be preferrable for large-scale installation. The method of foam application could also use additional consideration. The epoxy guns had far too low capacity and volume for what would be preferrable for large-scale installation. This forced us to refill the cartridges many times, adding significant time and difficulty to the

installation process. With our application system, we found it very difficult to completely fill every support, and many were left with gaps and imperfections.

To test the feasibility and effectiveness of our design, we installed our experimental solution in a single lane on the eastern side of the SR 520 Bridge. Because most vehicles drive in the center of the lane, there are clear markings where the two tires of each car most commonly strike the edges of the MEJ beams. To reduce installation time and production cost, we installed 2-ft supports only in these positions where tires commonly strike (Figure 4-3.A). While most cars successfully passed over the supports, additional post processing was required to manually select cases in which vehicles partially missed the supports.

Because of several design and roadway inconsistencies, our support installation had to be completed over multiple steps. Upon installation, the height of the chevron structures extended above the surface of the roadway. Overhead traffic destroyed some of them completely and damaged most of the others. Even with the opposing chevron design, many of the supports could also be seen to have “walked” transverse to the movement of the bridge, which indicated failure of the support-beam adhesion. Additionally, the extra height created an uneven road surface, and the supports did little to improve MEJ noise. Despite this failure, we were able to return to the bridge and replace some of the destroyed supports, attempt to mend the others, and shave down the extra height to create a smooth road surface. In replacing the chevrons care had to be take in order not to cut into the seal below. Returning to the bridge and completing these updates instantly made an audible difference in MEJ noise and resolved the “walking” that we had observed before.

Unfortunately, because of this error, many of the joints were structurally compromised upon test initialization. We expect this to greatly affect overall structure durability over time. The new supports that we installed to replace destroyed sections are the only non-damaged components and may offer a better indication of how the structure will survive over time. We performed this renovation completely at night, and temperatures were colder than suggested to correctly cure the Bostik flexible adhesive. Because this was a short road closure, the glue also had only approximately 4 hours to cure instead of the desired 24 hours before traffic began driving over the lane. We believe that improper curing of the adhesives will affect the overall performance and durability of the structure.

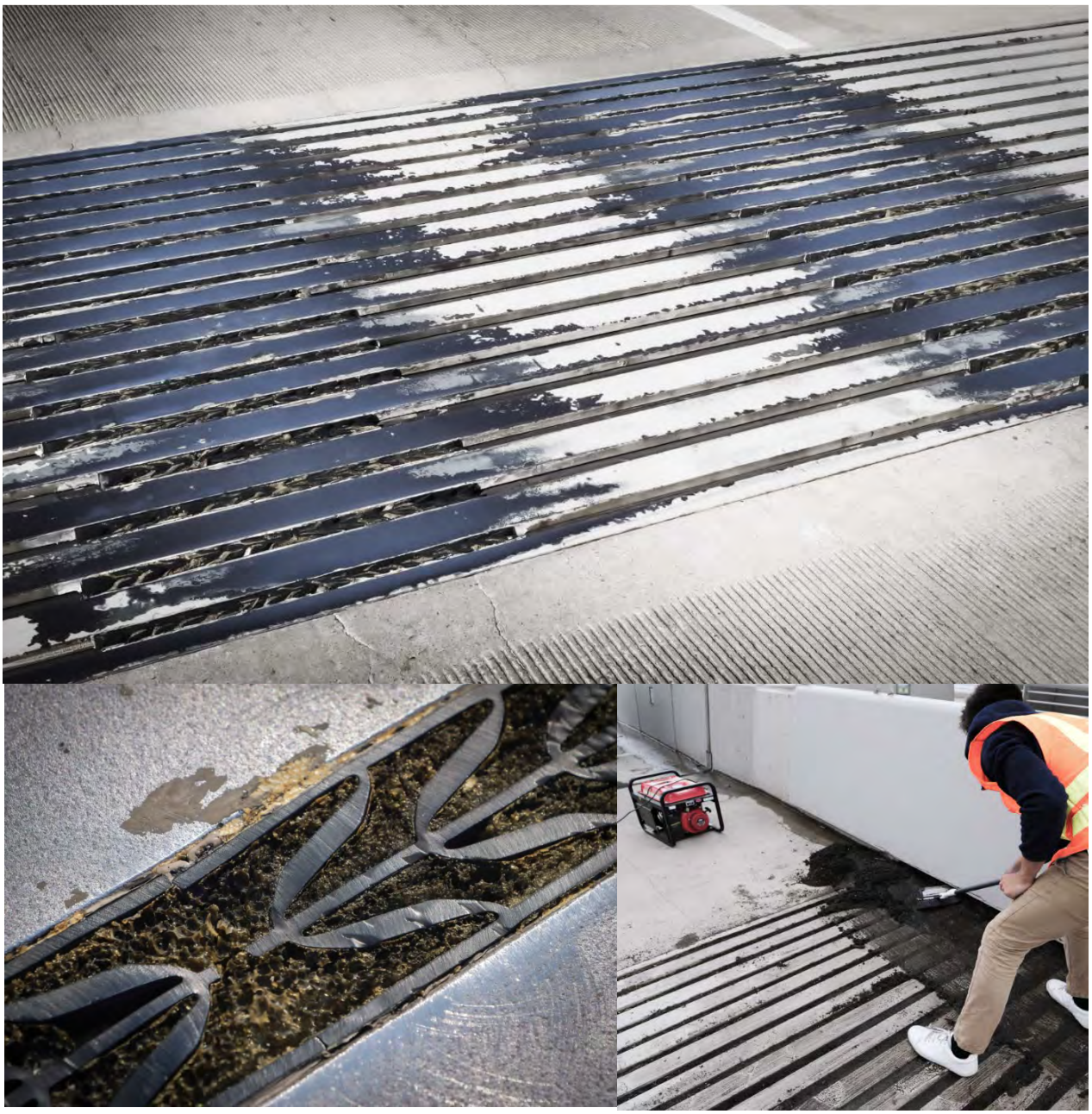

Figure 4-3. Installation of MEJ treatment. A, B) Support structure after four weeks of wear. C) Cleaning out the expansion joint before installation.

Five days after the supports had been adjusted, we once again returned to the MEJ and installed 3-in. by 4-in., 3.5-lb density viscoelastic (memory) foam extrusions into the spaces between each I-beam, below the moisture seal. Although this foam was not included in the original single-layer design, we wanted to evaluate whether including a viscoelastic dampening material between the beams would improve results. We hypothesized that additional foam could possibly

reduce either the remaining low-frequency noise from the MEJ beam structure or reduce any amplification that could occur from the chamber below the MEJ. We filled every gap in the MEJ and spanned a width approximately equal to that of the single lane. To install this foam, we squeezed it into the space between the beams, where it expanded to fill the gap and remained secured through mechanical interference (Figure 4-4). As shown by the initial results (figures 4-5, 4-6), the foam did little to reduce the noise of the MEJ. These results could be potentially improved by filling the entire span of the bridge, but additional investigation would be required to evaluate the potential benefits of this procedure.

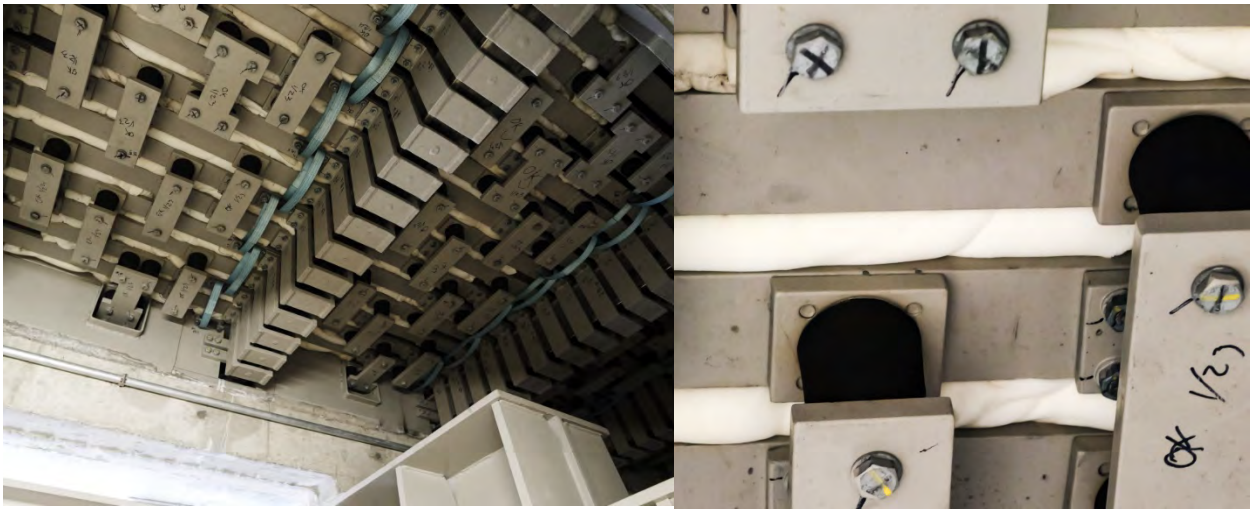

Figure 4-4. Underside of the MEJ with viscoelastic foam strips stuffed into the gaps.

4.2 Initial Results

To evaluate the performance of the support structure, we took control audio readings before the initial installation. We recorded 90 seconds of audio roadside directly in line with the MEJ and 90 seconds of audio roadside 160 feet in front of the MEJ. At both distances, the impact of the car tires striking the MEJ resulted in two distinct peaks, one as the front tires rolled over the joint and the second as the rear tires passed. Each 90-second sample contained many viable test events in which a vehicle struck the supported lane of the MEJ with no other vehicles present. Details of post processing can be found in section 3.2. After the treatment had been installed, we returned to the MEJ roughly one hour after traffic started driving across the bridge to again take measurements. From observations, the pitch and the magnitude of the noise emitted from the supported section of

the MEJ was a lower frequency and quieter than the unsupported section (SM Video). At a distance of 160 feet in front of the joint, the noise from the supported lane became very difficult to discern from that of general roadway traffic (SM Video). We measured the overall ESD for both the control and the initial results for the support; additionally, we subtracted the background noise of roadway traffic directly before each event to show the contrast of the impact noise from the general noise of the bridge (figures 4-5, 4-6).

Figure 4-5. Map showing expansion joint and sound measurement locations.

As shown in figures 4-6 and 4-7, a significant spike in energy occurred between 500 Hz and 900 Hz for the control testing. These results mirror those presented by the findings in the UW's phase 1 *Modular Expansion Joint Noise Mitigation Study*[14]. As humans, we perceive this frequency range to be relatively loud in comparison to lower frequency signals, and shifting or diminishing this peak has been a primary objective for an effective solution. Both directly beside the MEJ and 160 feet in front of the MEJ, we saw significant reductions in broadband RMS, especially in the problem frequency region of 500 to 900 Hz. In the full spectrum 0- to 15000-Hz frequency range, we saw the most significant differences occur in the 0- to 1000-Hz frequency

range. Matching our qualitative observations, the sound recorded directly beside the MEJ changed less significantly with the installation of the supports than the sound recorded 160 feet in front of the MEJ. Comparing event recordings to background noise, we saw a 56.0 percent reduction in broadband RMS directly beside the MEJ and an 89.61 percent reduction in broadband RMS at 160

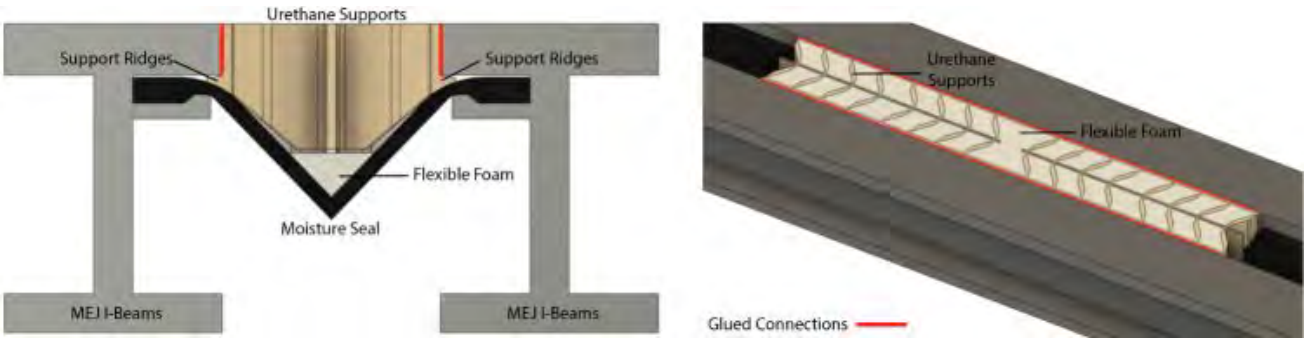

Figure 11. *Diagram detailing support installation components.*

feet in front of the MEJ. It should be noted that the peak at the 500 to 900 Hz interval was reduced by approximately 10 dB. At a distance farther than 160 feet the effective noise attenuation made it difficult to distinguish between general roadway noise and the noise from the supported expansion joint. As a result, accurate post processing became very difficult, and we could not clearly select events since the other lanes with untreated expansion joints were also open to traffic.

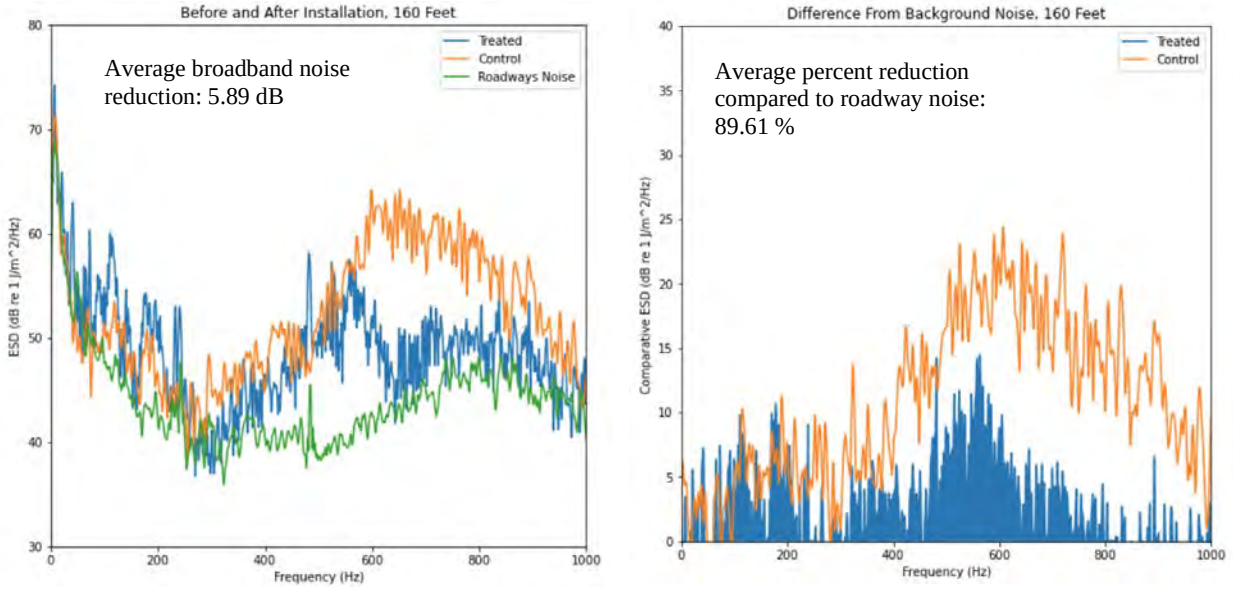

Figure 4-6. Comparison between control and initial results at a distance of 160 feet.

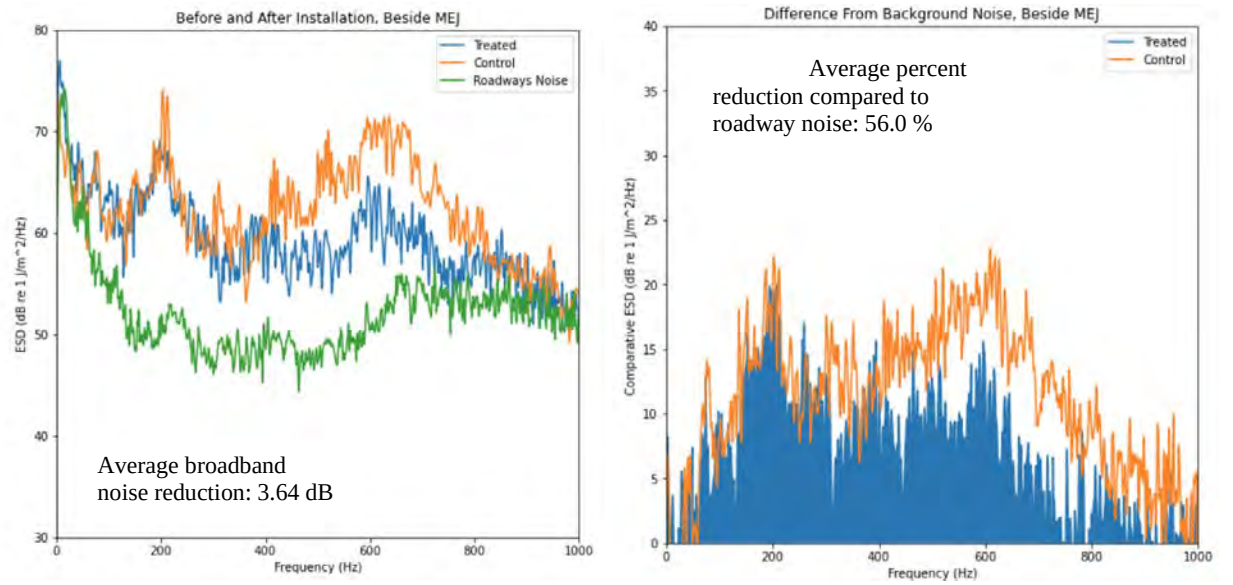

Figure 4-7. Comparison between control and initial results directly beside the MEJ.

4.3 Performance Over Time

We took measurements at the MEJ pre- and post-support installation, before and after inserting additional foam below the moisture seal (five days), and then every two weeks for two months. Changing environmental and road conditions existed for each measurement, possibly

resulting in some inconsistencies in the data. Over the period of two months (September to October), the average span of each gap in the expansion joint increased significantly (approximately 1.5 in. to approximately 2.5 in.), and temperature and humidity varied greatly day to day. Given simulation results, we expect a widening gap to corelate to an increase in MEJ noise, but no physical data exist to validate this assertion. Additionally, roadway traffic played a role in both background noise and average vehicle speed (i.e., more traffic tended to correlate to slower speeds). To help account for this, we subtracted the background noise from the expansion joint noise to give us the overall noise contribution of the impacts (see details in section 3. Methodology).

Comparing the difference between the supported MEJ section and the control allowed us to observe general trends in the performance of the MEJ treatment over time. As shown in Figure 4-8, directly after installation at a distance of 160 feet, the difference between standard roadway noise and supported MEJ was less than 1 dB, which is generally considered imperceptible[18]. Throughout the entirety of testing, the difference in sound levels remained below 2 dB, which is considered to be barely perceptable[18]. At these levels, the surrounding neighborhood would experience no perceivable difference in noise between the bridge roadway and the expansion joint.

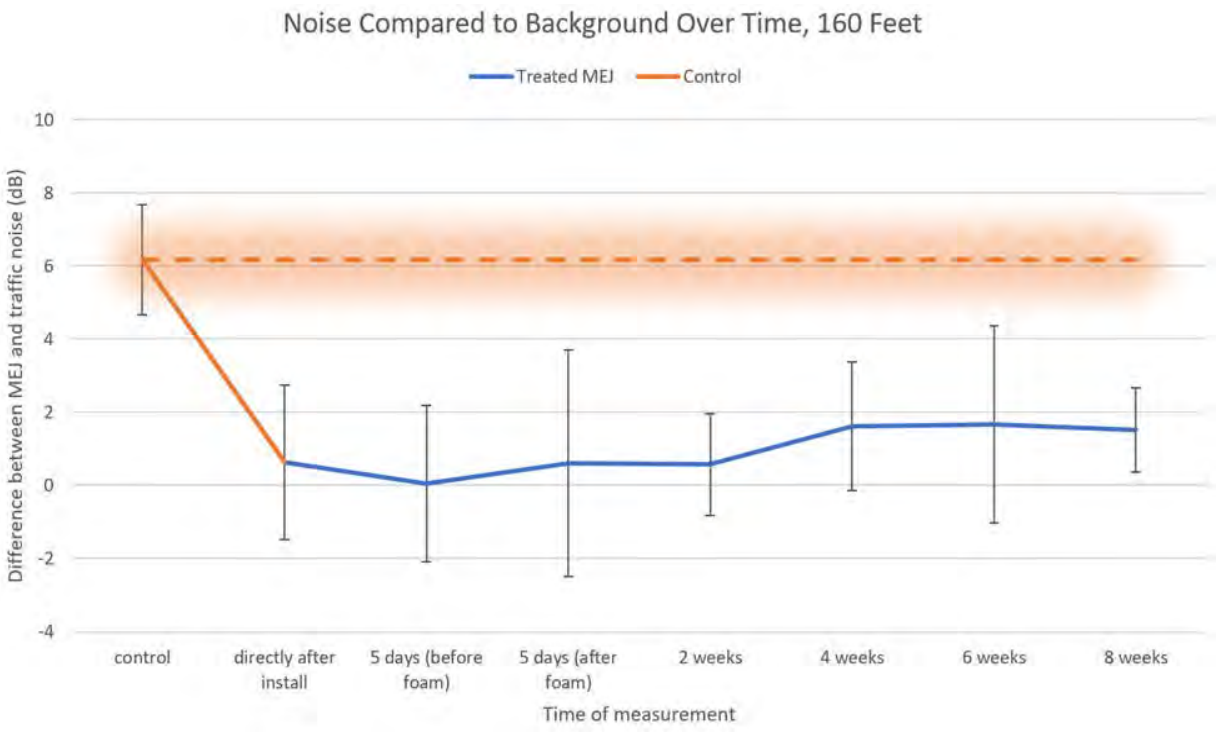

Figure 4-8. Comparison between roadway noise and MEJ noise over a two-month period at a distance of 160 feet. Error bars represent standard deviation of measurements.

As shown in Figure 4-9, the noise directly beside the MEJ was significantly more noticeable but still greatly improved from the original configuration. With no support, the difference between MEJ and roadway noise was over 8 dB, which is fairly close to the 10-dB threshold that generally denotes double the perceived noise level[18,19]. Throughout the duration of the study, the noise of cars driving over the supported expansion joint increased but remained well below the noise of the original control testing.

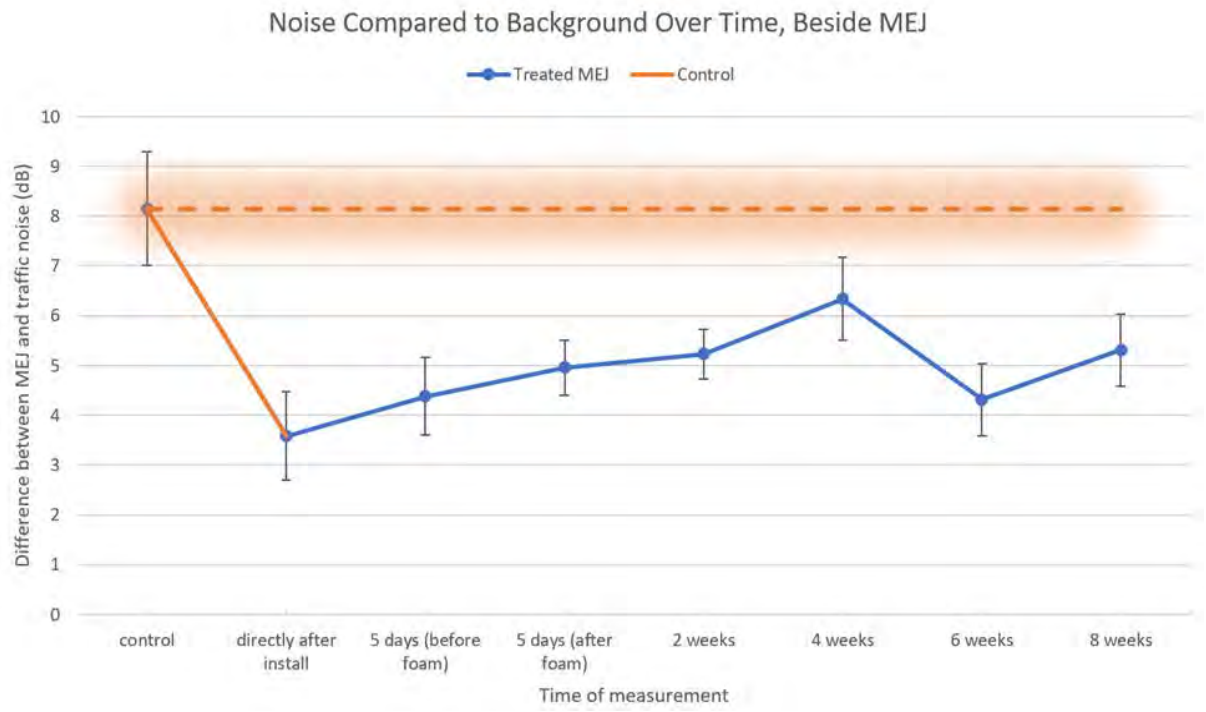

Figure 4-9. Comparison between roadway noise and MEJ noise over a two-month period directly beside the MEJ. Error bars represent standard deviation of measurements.

To get a sense for performance over time, we calculated the percentage of audible noise reduction.

$$\%\ Reduction = \frac{(RMS_c - RMS_{rc}) - (RMS_s - RMS_{rs})}{(RMS_c - RMS_r)}$$

Here RMS_c is the noise in dB of the control MEJ, RMS_{rc} is the noise of the road in front of the control MEJ, RMS_s is the noise of the supported MEJ, and RMS_{rs} is the noise of road in front of the supported MEJ. As seen in figures 4-8,4-9, and 4-10, the MEJ treatment performed best during the first two weeks of implementation at both 160 feet and directly beside the MEJ. Between week 2 and 4 we observed a slight increase in MEJ impact noise. From week 4 to week 8, we measured some variation in treatment noise but observed no clear trend in the data. Throughout the two-month period, noise measurements remained lower than that of the sinus plate at both distances.

Figure 4-10. Comparison between untreated MEJ noise and the installed treatment over a two-month period at a distance of 160 feet.

Approximately four weeks after installation, we closely inspected the supports during a scheduled bridge closure. First, we observed the rubber supports to be in roughly the same condition as when we initially trimmed their height after installation. Supports that had been damaged within the first few days of installation remained in place, but some of the glued connections appeared to have failed, and the flexible joints appeared severely compromised. In contrast, the replacement supports that had been trimmed flat at the time of installation remained in exceptionally good condition. In many of the supports, the foam also experienced significant wear. This likely occurred because of a combination of imprecise application of the foam during installation and wear of the soft material. The previously damaged supports appeared to show a more pronounced loss of foam (Figure 4-11) than the intact replacement joints (Figure 4-3). We also noted deposition of large amounts of gravel inside the MEJ gaps since we had cleared out debris four weeks earlier (Figure 4-11). While this was clearly apparent in the spaces with no added treatment (Figure 4-11), the gaps within supports themselves had virtually no build-up of debris.

Figure 4-11. Over one month of installation, gravel and debris started to fill up the unsupported portion of the joint (left), while we observed no debris in the chevrons themselves. While the chevrons remained in good condition, some foam had been pulled from the supports after one month of wear (right).

4.4 Suggestions for Future Implementation

Future work should consider several design and installation aspects for large-scale implementation. First, we conducted this study with convenient fabrication processes and materials for rapid prototyping and low run production. While we selected effective support materials for testing functionality, more durable options may be available by using another fabrication process such as injection molding, which we avoided because of cost, low part counts, and time restrictions. To fabricate each 2-ft support section, we glued together four individual 6-in. components. While this was strong enough for installation, more permanent methods may exist to fuse components. The foam we used was an off-the-shelf, two-part mixture that was in no way optimized for extended use in an outdoor environment. For enhanced durability, a more specialized foam may be desired. While the chevron supports offer the foam some protection from vehicle wear, ideally, the foam would sit slightly shy of the road's surface, and an additional coating would be added to improve weathering and abrasion resistance.

We performed the one-lane installation of the treatment in approximately two 9-hour sessions with two people continuously working. With improved methods, the time required for this process could be dramatically reduced. Initially, we spent several hours cleaning debris out

the joint, a step that could be performed ahead of time in much less time by using the proper equipment. Next, sizing inconsistencies in the interior of the beam gaps between the moisture seal and the beam forced us to trim several of the chevron supports by hand to ensure a tight fit. Adjusting the support geometry to universally fit in every gap or using a more specialized tool for trimming the support would dramatically improve installation time. When gluing the support structure to the MEJ beams, we relied on the rebound of the compliant structure to hold the support in place as the glue cured. Many of these supports didn't create adequate pressure to squeeze excess glue from the interface, and an additional specialized tool to expand the support might have improved adhesion. Properly curing the Bostik flexible adhesive takes a minimum of 24 hours in warm, dry weather. Special care should be taken to ensure that weather conditions and installation timelines match these requirements. The support structures can be removed from the expansion joint by sliding a knife along the glued interface between the joint and the I-beam and pulling them out with a pair of pliers. Caution should be exercised to not damage the seal below.

This study showed that the chevron system is a very effective means of significantly decreasing the noise emanating from large expansion joints. To examine the long-term durability on an installed system we propose the following next phase:

1) Installation of the chevron system across all westbound lanes of east SR 520 expansion joint.
2) Injection molding of the chevrons to decrease the cost of larger volume fabrication.
3) Use of high durability material consisting of a mix of natural rubber, synthetic rubbers, and antioxidants instead of high strength urethane.
4) Use of fiber-reinforced, low density foam with a high strength polymer as a protective layer.
5) Inspection for wear and acoustic performance every month for up to one year with modifications as needed.
6) Full installation across all lanes of the east expansion joint of the SR 520 bridge if the wear characteristics are judge satisfactory,

4.5 Conclusions

This study investigated the design and feasibility of noise mitigation strategies for installation in modular expansion joints (MEJs), with a focus on Washington state's SR 520 bridge.

The three main sources of noise from the MEJ include resonance of the air within the gaps, resonance of the beams, and resonance of the tires. By filling the gaps in the MEJs with a supportive zero-Poisson's ratio material, we can reduce the input signal for each of these noise sources simultaneously. We proposed two potential solutions to reduce tire deformation into beam gaps and subsequently decrease pressure spikes on tires and beam edges: a single-layer support structure, and a multi-layer support structure. We performed both physical testing and simulation to evaluate the effectiveness of each solution and selected the single-layer chevron support to be the most feasible solution.

Installation of this treatment in one lane of the SR 520 bridge MEJ proved to be highly effective over the two-month test period. At a distance of 160 feet, we consistently measured a greater than 4.51-dB broadband reduction in expansion joint noise. This accounts for more than a 70 percent reduction in additional noise produced by the expansion joint over the background noise of vehicles on the flat roadway. Beyond 160 feet the difference in noise between the flat roadway and the MEJ became so small that it was difficult to accurately measure.

If these supports were installed in all expansion joints on the bridge, residents living in the area would still hear the general noise of the roadway, but the abrasive sound of vehicles hitting the expansion joints would effectively be eliminated.

While we showed that the chevron system can be an effective solution to the expansion joint noise issue, this report outlines further development and testing to extend the durability of the treatment.

References

1. *Tailor Made Concrete Structures: New Solutions for our Society (Abstracts Book 314 pages + CD-ROM full papers 1196 pages)*. (CRC Press, 2008). doi:10.1201/9781439828410.

2. Ding, Y., Zhang, W. & Au, F. T. K. Effect of dynamic impact at modular bridge expansion joints on bridge design. *Eng. Struct.* **127**, 645–662 (2016).

3. Bohatkiewicz, J., Jukowski, M., Hałucha, M. & Dębiński, M. Influence of the Acoustic Cover of the Modular Expansion Joint on the Acoustic Climate in the Bridge Structure Surroundings. *Materials* **13**, 2842 (2020).

4. Mao, D. & Ding, Y. Measurement and analysis of bridge expansion joint noise. *E3S Web Conf.* **293**, 02053 (2021).

5. Ravshanovich, K. A., Yamaguchi, H., Matsumoto, Y., Tomida, N. & Uno, S. Mechanism of noise generation from a modular expansion joint under vehicle passage. *Eng. Struct.* **29**, 2206–2218 (2007).

6. Ancich, E. J., Brown, S. C. & Cove, L. Modular Bridge Joints – Reduction of noise emissions by use of Helmholtz Absorber. 12.

7. Numerical investigation of noise generation and radiation from an existing modular expansion joint between prestressed concrete bridges | Elsevier Enhanced Reader. https://reader.elsevier.com/reader/sd/pii/S0022460X09005872?token=8E6C0FB3B1BE998C4A8C12979C97576F146391BC30D4236346C0CC38D134BC3E20386B5A6C7ACD7CB63BDF8A82571D51&originRegion=us-east-1&originCreation=20221021203714 doi:10.1016/j.jsv.2009.07.016.

8. Review of Noise Reduction of the Highway Bridge Expansion Joints. https://ascelibrary.org/doi/epdf/10.1061/9780784484265.214.

9. Moor, G., Spuler, T. & Hoffmann, S. THE MODULAR EXPANSION JOINT – UPDATE ON WHAT CAN TODAY BE EXPECTED OF IT. 22.

10. Spuler, T., Moor, G. & O'Suilleabhain, C. Single gap expansion joints – an optimal solution for small deck movements. in 404–405 (2013). doi:10.2749/222137813806501803.

11. Spuler, T., Moor, G. & O'Suilleabhain, C. Expansion joints for ever longer, lighter bridges. 8.

12. Vancouver's Golden Ears Bridge Noise Assessment. *HGC Engineering* https://acoustical-consultants.com/casestudy/vancouver-golden-ears-bridge-noise-assessment/.

13. Vaitkus, A. & Vorobjovas, V. Traffic / Road Noise Mitigation under Modified Asphalt Pavements Traffic / road noise mitigation under modified asphalt pavements. in *6th Transport Research Arena* (2016). doi:10.1016/j.trpro.2016.05.446.

14. Reinhall, P. G. & Soloway, A. G. Expansion Joint Noise Mitigation Study. 55.

15. Crocker, M. J. *Handbook of Noise and Vibration Control*. (John Wiley & Sons, 2007).

16. *Springer Handbook of Acoustics*.

17. Virtanen, P. *et al.* SciPy 1.0: fundamental algorithms for scientific computing in Python. *Nat. Methods* **17**, 261–272 (2020).

18. DECIBEL (LOUDNESS) COMPARISON CHART | Galen Carol Audio | Galen Carol Audio. https://www.gcaudio.com/tips-tricks/decibel-loudness-comparison-chart/.

19. Ljunggren, F., Simmons, C. & Hagberg, K. Correlation between sound insulation and occupants' perception – Proposal of alternative single number rating of impact sound. *Appl. Acoust.* **85**, 57–68 (2014).

20. PROSPECT-TENSA-MODULAR-LR-ch-en.pdf.

Appendix A. High Speed Testing

Support Type:	Max Noise Magnitude:	Percent Reduction:
No Support	.0054	None
Rubber Support	.0034	37% reduction
Nylon Support	.0030	44% reduction

A-1. Top support structures. (Left) Chevron design features an S-shaped hinge to reduce internal stress. This allows the structure to be fabricated from a stiff material such as nylon. (Right) We fabricated the structure from a flexible material such high 90A urethane or thermoplastic polyurethane (TPU).

As a car tire rolls over a gap in the road, it affects the edge of the gap, creating a pressure spike and a resulting noise. To evaluate the acoustic and dynamic effect of top support structures, we built a high speed (60 mph) test set-up to measure pressure on the beam's leading edges and changes in recorded sound. At the widest span, a car tire will only deform roughly 1 cm into the gaps between the beams. This allowed us to build a simplified test set-up by gluing ¾-in. steel beams to the roadway and driving over them at 60 mph to get a general comparison of noise with different top supports.

Appendix B. Static Testing Procedures

B.1 Physical Tests

To validate our simulations and assess the potential of each multi-layer design, we built a static compression test set-up (shown in Figure B-1) with reconfigurable components and tested eight different configurations for support deformation and edge pressure. We used Fujifilm 70-350 psi Prescale pressure paper to determine edge pressure and an IFM diffuse light photoelectric distance sensor to measure deformation in the structure. On the physical MEJ, the largest tire deformations and subsequent impacts occur when the gap spans a larger distance. We positioned the I-beams accordingly to have a 3-in. gap, the maximum MEJ gap width within its normal working range.

We built the approach ramps from wood and performed our compression tests by driving a Ford Transit Connect cargo van over the set-up. Additional variation in vehicle type could be tested to provide a wider range of results. For this specific test, using a single vehicle enabled us to perform side by side comparisons of configurations and select the most effective solution.

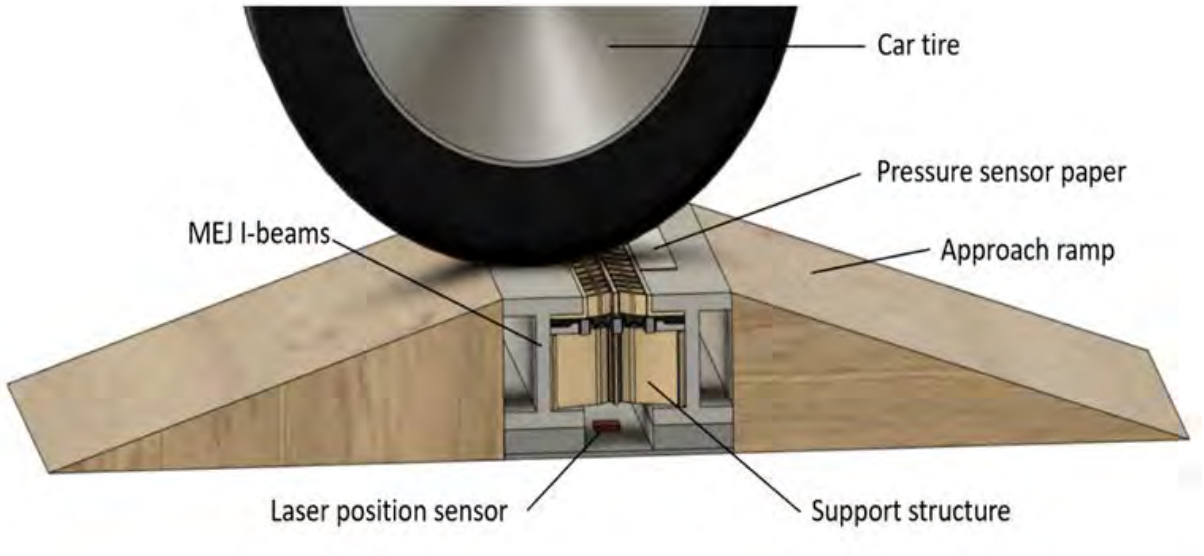

B-1. Compression test set-up. This test set-up matched a 2-foot section of the MEJ and could be driven over by a desired vehicle to provide pressure and displacement measurements.

We tested eight separate configurations (shown in Figure B.2.) to compare results for each individual support structure and combinations of support structures.

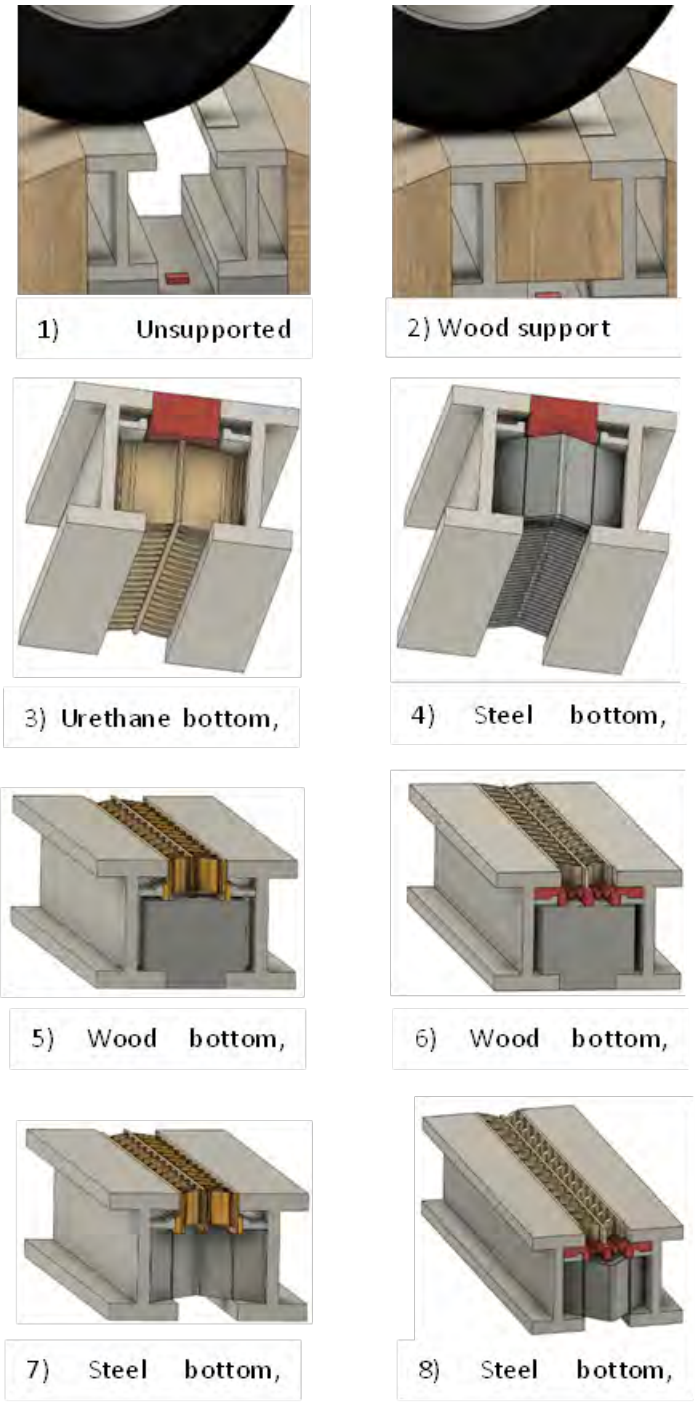

B.2. Compression test configurations 1 through 8. These include baseline testing, individual component testing, and full structure testing.

For baseline testing, we first performed tests with no support structure and a rigid support structure with very little deformation. To create the rigid support, we used layers of ¾-in. oak

planking cut to fill the gap. While this gave a good approximation of a flat surface, some compression still occurred in the wood, particularly at the interface of each rough surface. Next, we tested each of the four support structures individually by combining each with rigid supports as the other section of the structure. Inaccuracies in structure fabrication; dirt, gravel, and water on the roadway; and limited sensor accuracy all acted as sources of error in the tests.

To test deformation in the structure, we measured the distance from the lens to a fixed point on the surface of the structure by using the diffuse light position sensor and recorded the total displacement as a vehicle drove over the set-up. For the unsupported configuration we measured a total displacement of 9 mm, and for a quasi-rigid support made from oak we recorded a displacement of 0.7 mm. Each of the remaining six support configurations showed a dramatic reduction in deformation in comparison to the original gap. Samples 3, 4, 5, and 6 isolated individual support structures to give an idea of component-by-component rigidity. These tests demonstrated that spring steel lower-support greatly outperformed the urethane lower-support, with a total deformation of only 1.1 mm as opposed to 4.1 mm for the urethane version. The top supports both had relatively similar deformations, within the margin of error of the position sensor, but the plastic top support demonstrated a slightly lower deformation of 3 mm versus 3.6 mm for the rubber support. Configurations 7 and 8 tested the deformation of the combined multilayer structure, and both provided more than 60 percent reduction in overall deformation into the gap. Of these options, configuration 7 (spring steel lower support and rigid plastic upper support) offered the most resistance to deformation, showing a 65 percent reduction vertical of tire displacement.

To test the pressure on the leading edge of the I-beam, we used Fujifilm Prescale 70-350 psi pressure sensor paper, which chemically becomes a more vibrant shade of red under direct pressure. This sensing method offers instantaneous feedback and qualitative results but is difficult to quantify with a high level of confidence. We performed post processing on sample images to color code the results. As shown in Figure B.3., high pressures (350 psi) can be seen as bright orange areas, while low pressures (70 psi) show up as dark purple. The support solutions showed a dramatic reduction of pressure on the edge of the beam in comparison to the original unsupported sample. Some error could be found in these samples, since tiny pressure concentrations such as gravel or misalignment in support height also created small areas of high pressure.

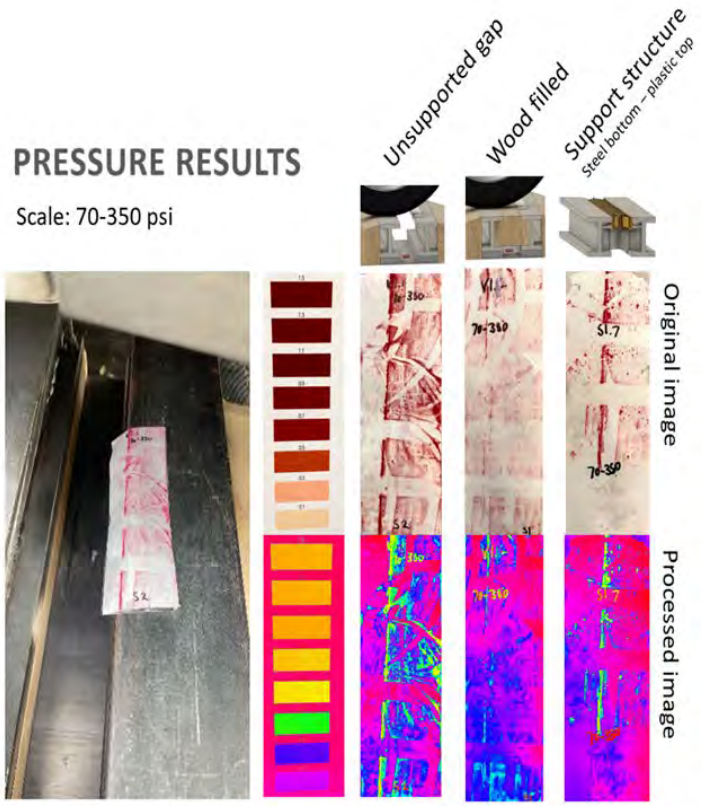

B.3. Pressure measurements for each test configuration. All supported configurations had noticeably lower pressure concentrations at the beam edge.

B.2 Simulation Results

Simulations of three test configurations (unsupported, rigid support, metal-plastic chevron support structure) are shown in Figure B.4. These results showed trends that were similar to our experimental results. Deformations shown in the simulation results were much lower than those observed in physical tests. Factors that may account for these discrepancies include inconsistent fabrication, compression in the rough surface to surface connections, and differences in tire size and material properties. All test results indicated a significant reduction in pressure on the beam edges, leading to a reduction in excitation energy and noise. The support structure simulations showed a 69 percent reduction in maximum pressure on the beam and showed only a 30-psi pressure increase from the flat, rigid surface simulation.

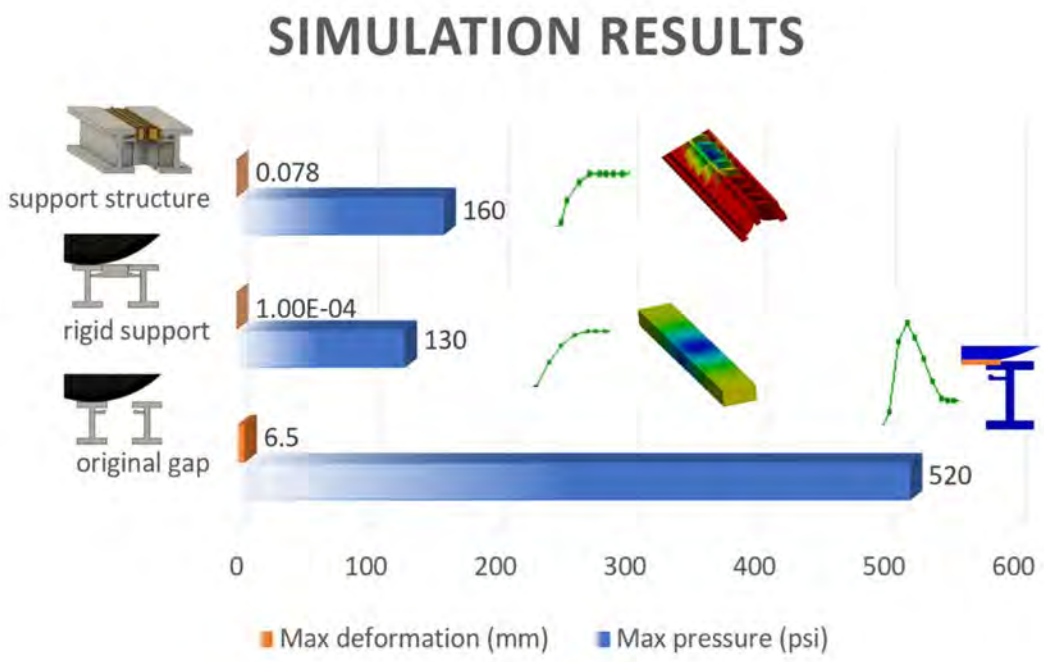

B.4. Pressure and deformation results from finite element simulations of each configuration. Icons show the pressure profile as it impacts the beam, with green being maximum pressure, blue being average pressure, and red being minimum pressure. The pressure curves (shown in green) show the maximum pressure on the I-beams.

Appendix C. Full 520 Bridge MEJ Test Results

C.1 Roadside Test Results

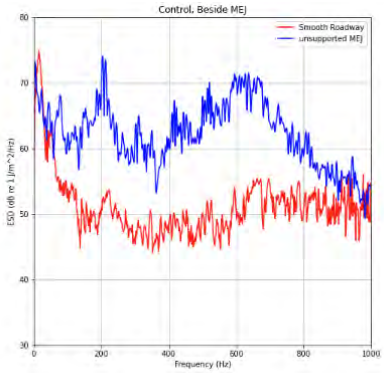

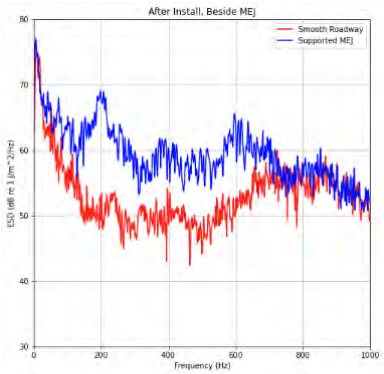

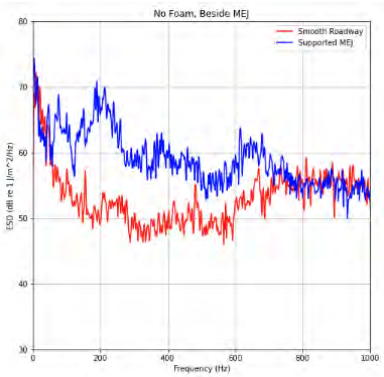

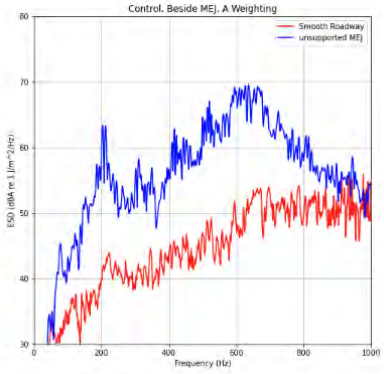

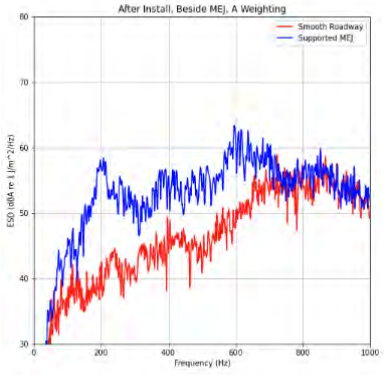

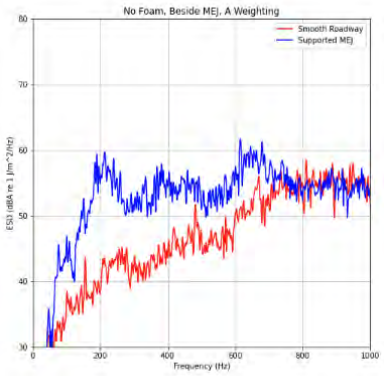

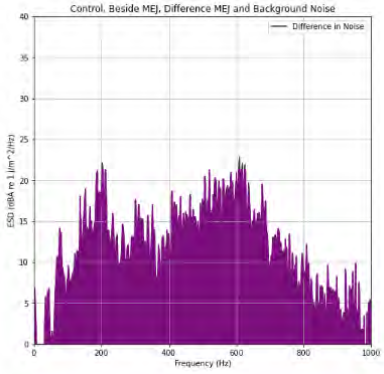

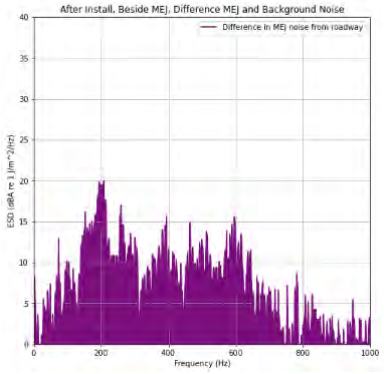

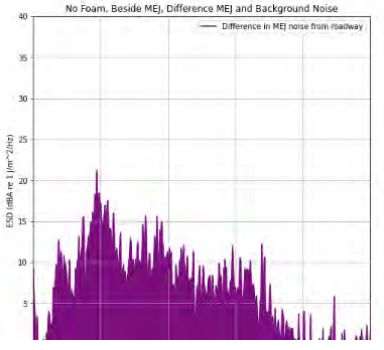


```
road rms:
avg rms 93.00629235337709 +/- 2.442946488180547 dB

support rms:
avg rms 101.15208665312284 +/- 1.1401473468784902 dB
```

```
road rms:
avg rms 93.92484797024257 +/- 1.5159582590966658 dB

support rms:
avg rms 97.51196025973033 +/- 0.893676275102695 dB
```

```
road rms:
avg rms 92.80165650856223 +/- 1.4778772848731931 dB

support rms:
avg rms 97.18083259514447 +/- 0.7879023141340654 dB
```

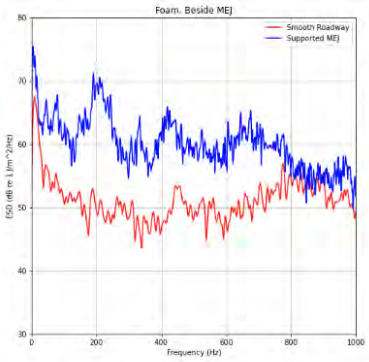

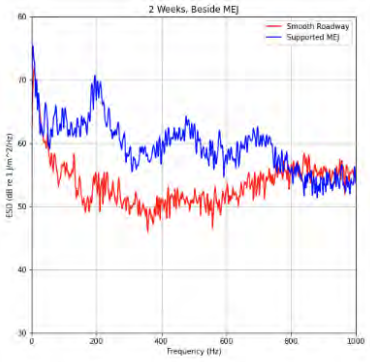

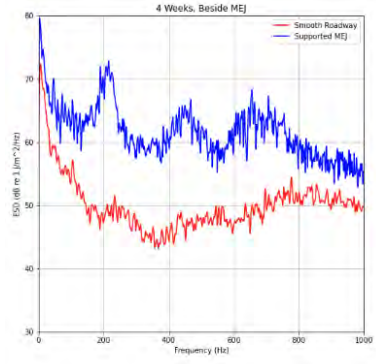

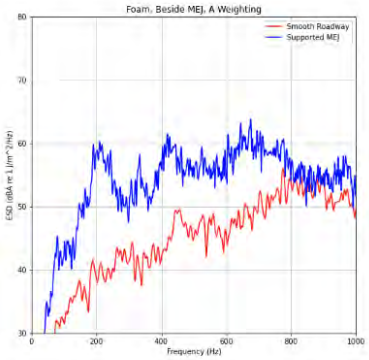

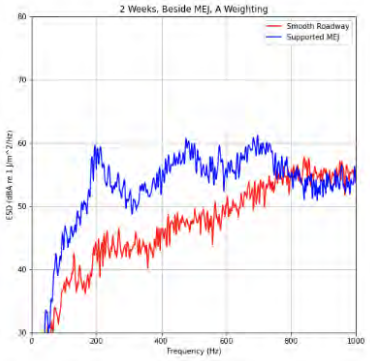

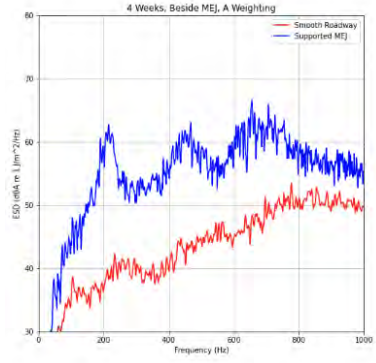

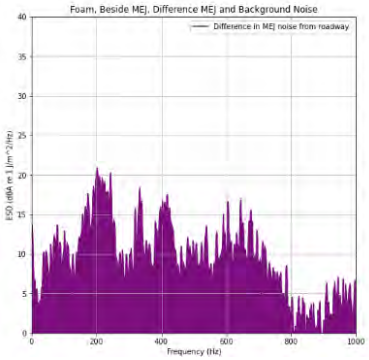

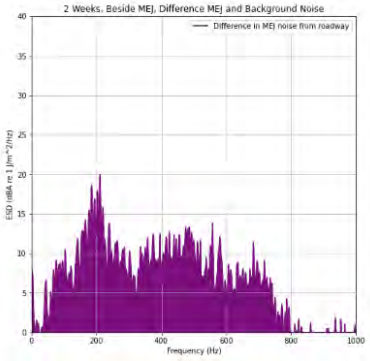

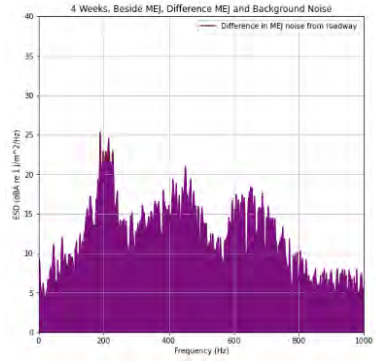


```
road rms:
avg rms 93.13054991415008 +/- 0.9981218000406752 dB

support rms:
avg rms 98.08902735686293 +/- 0.5587382244214214 dB
```

```
road rms:
avg rms 92.9784894659716 +/- 0.8200706499253699 dB

support rms:
avg rms 98.20932119395796 +/- 0.5005160130297738 dB
```

```
road rms:
avg rms 92.23218315995246 +/- 0.9830175071969608 dB

support rms:
avg rms 98.5733725881718 +/- 0.8313370953019971 dB
```

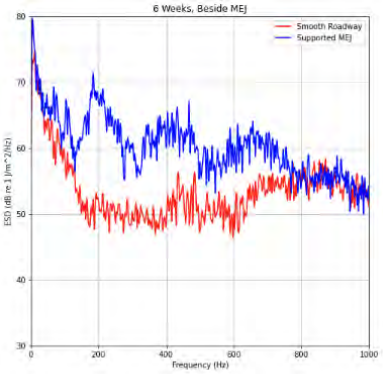

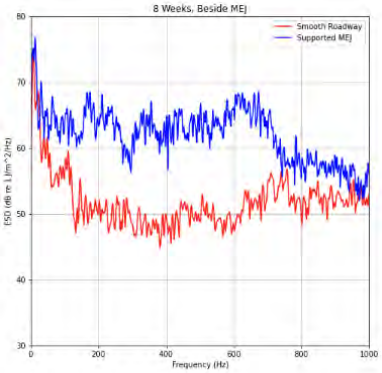

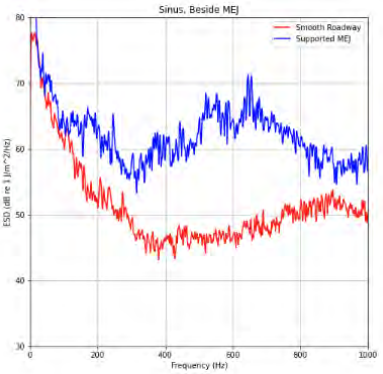

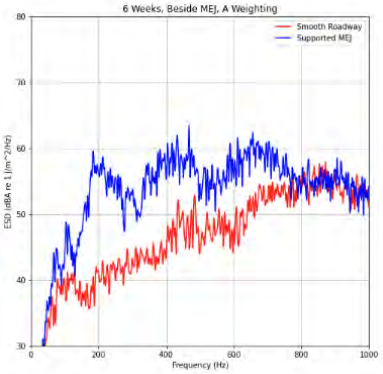

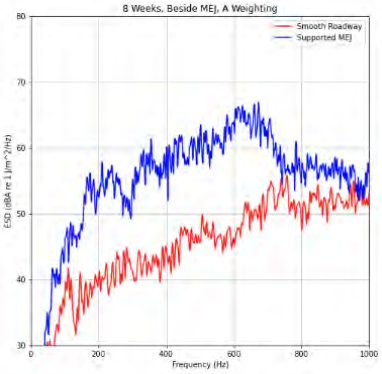

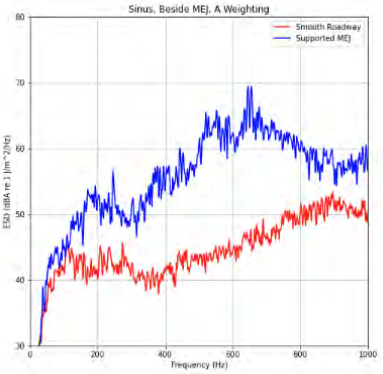

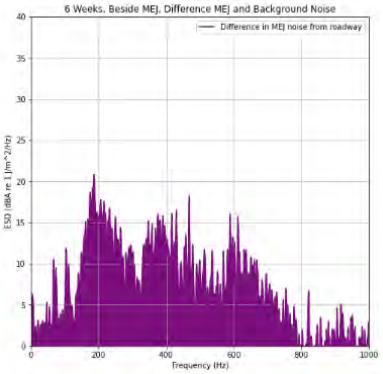

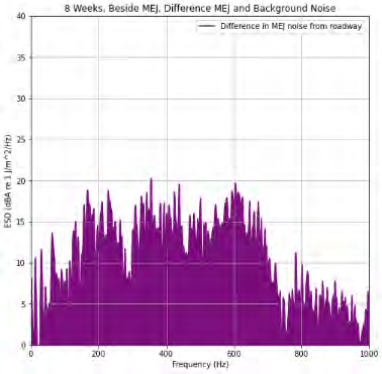

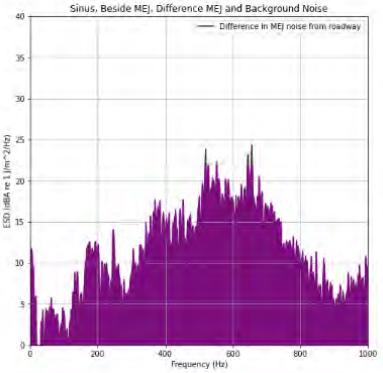

road rms:
avg rms 94.20808391359218 +/- 1.8436229451646244 dB

support rms:
avg rms 98.52223762479328 +/- 0.7300707601836331 dB

road rms:
avg rms 93.35091844097164 +/- 1.2817754440141105 dB

support rms:
avg rms 98.66089342799323 +/- 0.7201799666430807 dB

road rms:
avg rms 97.29270578713043 +/- 1.3421456498739521 dB

support rms:
avg rms 103.68620913171071 +/- 1.6844597050176147 dB

C.2 Test Results at 160 Feet

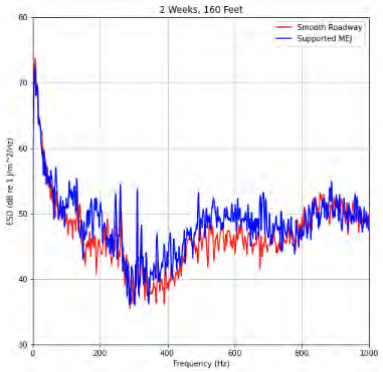

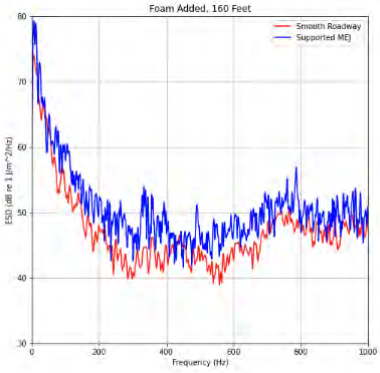

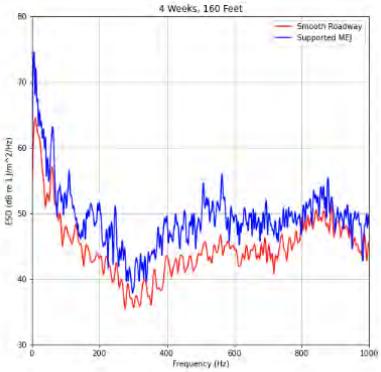

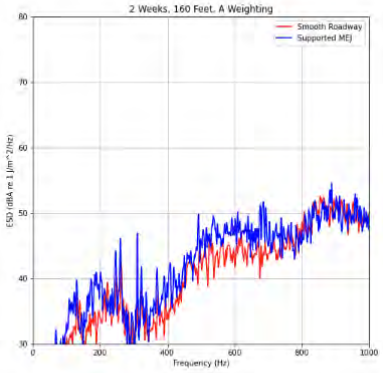

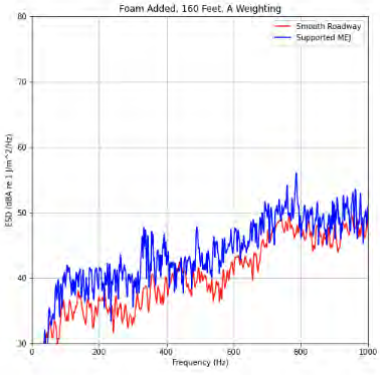

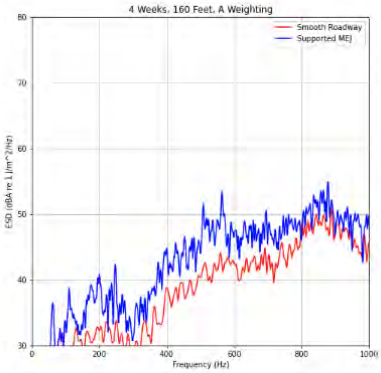

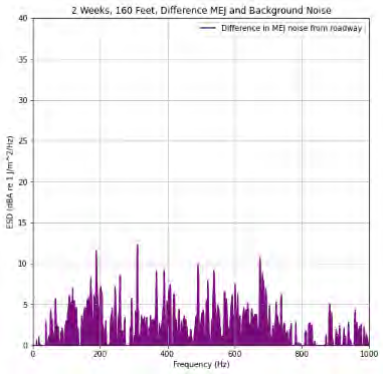

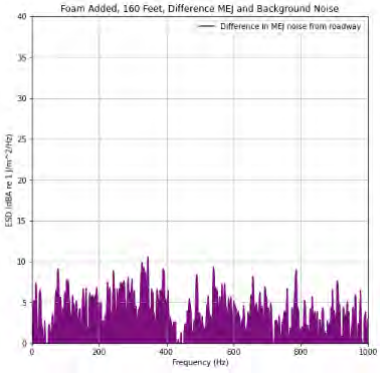

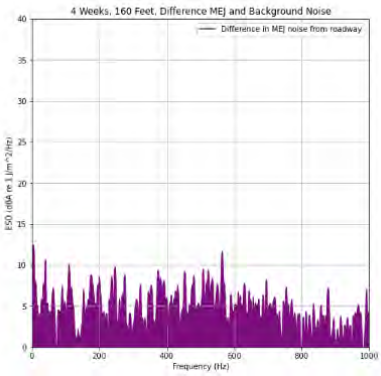


```
road rms:
avg rms 92.98971959105067 +/- 2.3022513364087605 dB

support rms:
avg rms 93.60011778239631 +/- 3.0744470248568687 dB
```

```
road rms:
avg rms 89.06865647608726 +/- 1.5050269448549545 dB

support rms:
avg rms 90.70466665674218 +/- 1.7592174919765862 dB
```

```
road rms:
avg rms 88.54932311386182 +/- 2.008925246340456 dB

support rms:
avg rms 87.9697272402375 +/- 1.3975977083687727 dB
```

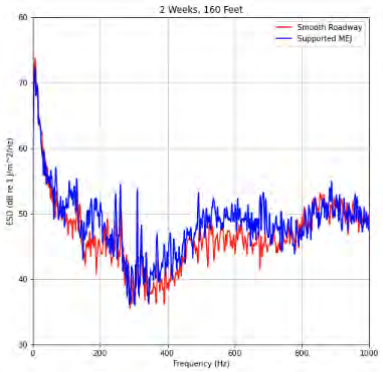

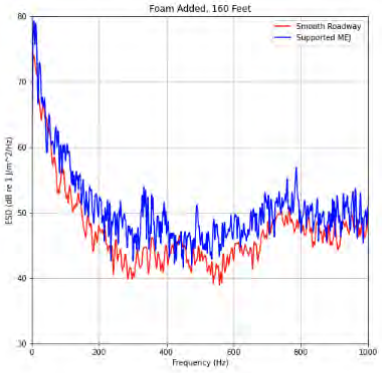

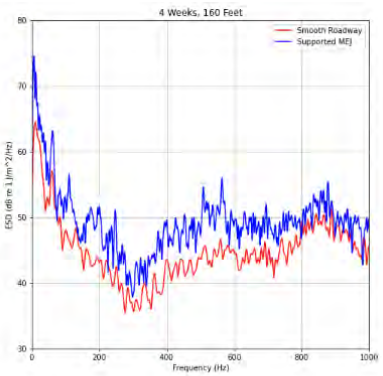

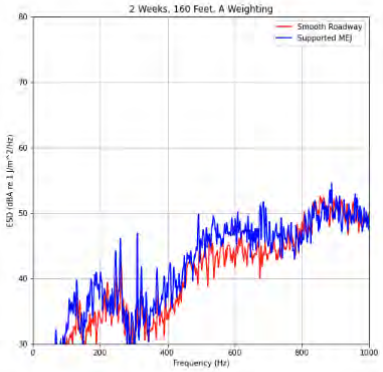

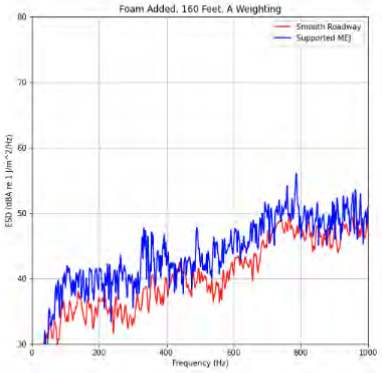

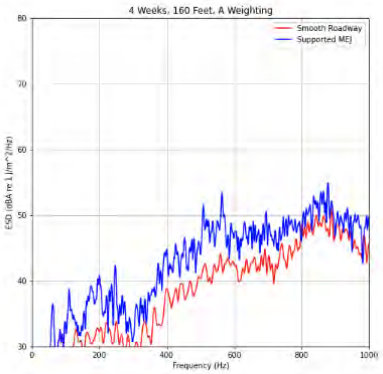

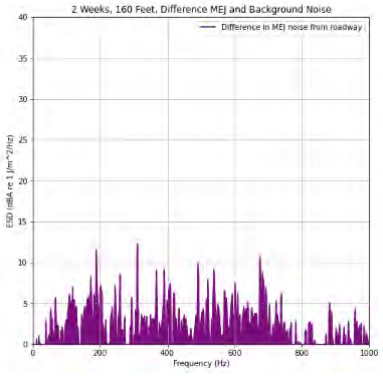

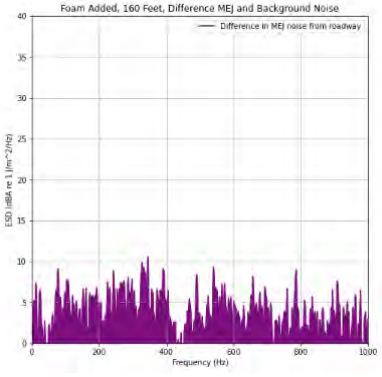

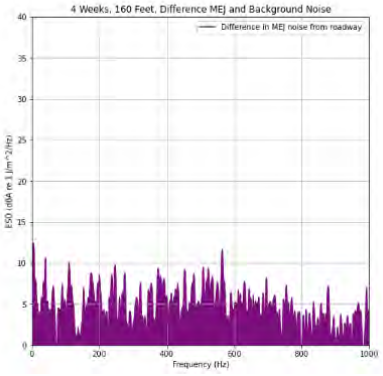

road rms:
avg rms 92.98971959105067 +/- 2.3022513364087605 dB

support rms:
avg rms 93.60011778239631 +/- 3.0744470248568687 dB

road rms:
avg rms 89.06865647608726 +/- 1.5050269448549545 dB

support rms:
avg rms 90.70466665674218 +/- 1.7592174919765862 dB

road rms:
avg rms 88.54932311386182 +/- 2.008925246340456 dB

support rms:
avg rms 87.9697272402375 +/- 1.3975977083687727 dB

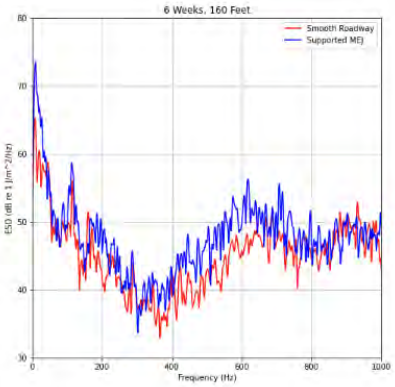

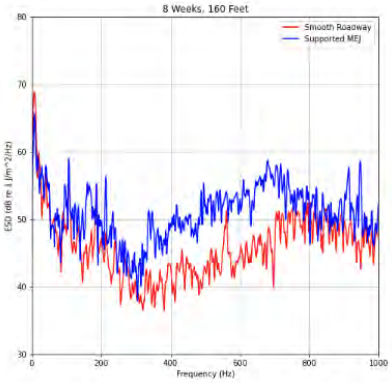

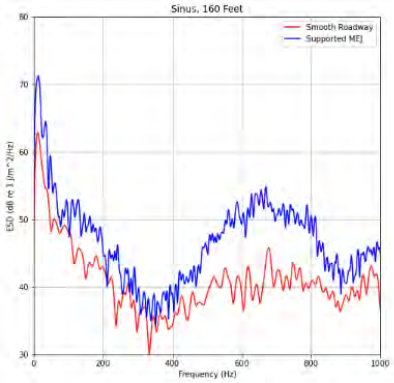

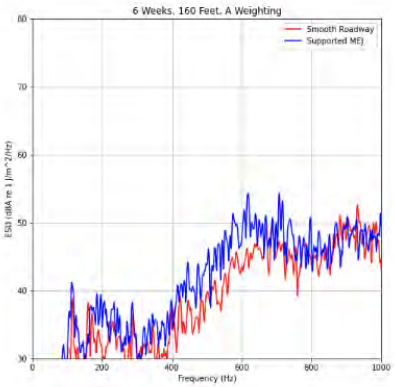

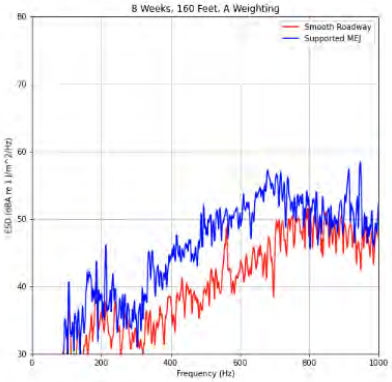

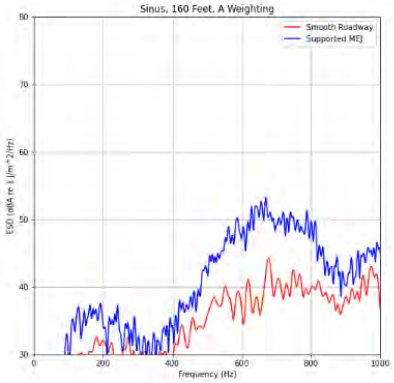

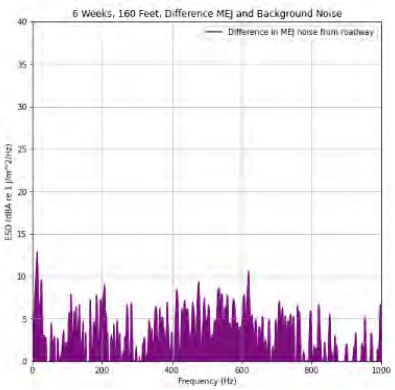

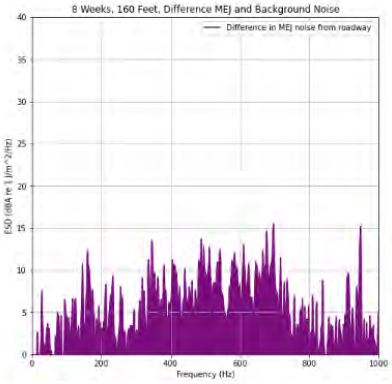

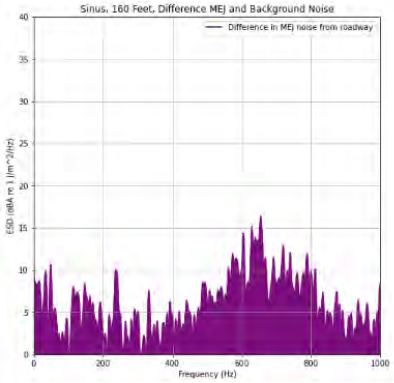

road rms:
avg rms 87.37330979053705 +/- 1.8443004144446955 dB

support rms:
avg rms 89.03812348557146 +/- 2.7026584266780254 dB

road rms:
avg rms 87.24628409845741 +/- 2.736960746858909 dB

support rms:
avg rms 88.76852168976542 +/- 1.1542263129304955 dB

road rms:
avg rms 86.36323853190031 +/- 1.8840942972315275 dB

support rms:
avg rms 90.63011650698735 +/- 2.073780639479017 dB